

Review

Research Progress on the Wear and Corrosion Resistant Plasma Electrolytic Oxidation Composite Coatings on Magnesium and Its Alloys

Chen Zhao ¹ , Xingwei Wang ^{1,2}, Bo Yu ^{1,2}, Meirong Cai ^{1,2}, Qiangliang Yu ^{1,2,*} and Feng Zhou ²¹ Shandong Laboratory of Yantai Advanced Materials and Green Manufacturing, Yantai 264000, China² State Key Laboratory of Solid Lubrication, Lanzhou Institute of Chemical Physics, Chinese Academy of Sciences, Lanzhou 730000, China

* Correspondence: yql@licp.cas.cn

Abstract: Plasma electrolytic oxidation (PEO), as a cost effective and environmentally friendly technology, has been applied on magnesium and its alloys to improve wear and corrosion resistance. Additionally, combining with particles addition in the electrolyte and/or various post-treatments could diminish the intrinsic structural defects of the PEO coatings and provide multifunctionalities, including wear resistance, corrosion resistance, self-lubrication, and self-healing. This paper reviews recent progress on PEO composite coatings prepared by in situ incorporation of functional particles and/or post-treatments on magnesium and its alloys. The focus is given to the microstructural and functional changes of the PEO coatings, particularly on the wear and corrosion behaviors.

Keywords: plasma electrolytic oxidation; magnesium; composite coating; wear; corrosion



Citation: Zhao, C.; Wang, X.; Yu, B.; Cai, M.; Yu, Q.; Zhou, F. Research Progress on the Wear and Corrosion Resistant Plasma Electrolytic Oxidation Composite Coatings on Magnesium and Its Alloys. *Coatings* **2023**, *13*, 1189. <https://doi.org/10.3390/coatings13071189>

Academic Editor: Maria Vittoria Diamanti

Received: 3 June 2023

Revised: 24 June 2023

Accepted: 29 June 2023

Published: 1 July 2023



Copyright: © 2023 by the authors. Licensee MDPI, Basel, Switzerland. This article is an open access article distributed under the terms and conditions of the Creative Commons Attribution (CC BY) license (<https://creativecommons.org/licenses/by/4.0/>).

1. Introduction

Magnesium and its alloys stand out as one of the lightest engineering materials with high strength-to-weight ratio, good electromagnetic shielding, high damping capacity, and efficient machinability [1–3]. Consequently, these materials have found widespread applications in aerospace, automobile, computer, communication, and consumer electronics sectors. However, their high chemical activity and low hardness limit their performance, highlighting a need for surface treatments to improve the wear and corrosion resistance [4,5]. Various techniques have been established for the surface modification of magnesium and its alloys, including conversion coatings, electroplating, electroless plating, anodizing, plasma electrolytic oxidation, physical/chemical vapor deposition, organic coatings, and sol-gel technique [6–23].

Plasma electrolytic oxidation (PEO), also known as micro-arc oxidation (MAO), is an affordable and environmentally friendly technique. The PEO process is associated with discharges, which were generated under a strong electric field across the metal-electrolyte interface. Generally, this interface consists of the metal substrate, the oxide film, a gas envelope, and the electrolyte. Plasma assisted chemical reactions occurred with the discharges and at the areas nearest the discharges. Thus, the substrate metal was converted into a compound, comprising the metal itself, oxygen, and the electrolyte components. For instance, coatings formed in silicate electrolyte usually consist of MgO, MgSiO₃ and MgSiO₄; coatings formed in phosphate electrolyte might contain Mg₃(PO₄)₂; coatings formed in aluminate electrolyte comprising MgO and MgAl₂O₄. MgF₂ could also be produced when fluoride ions are introduced to the electrolyte. Several models were proposed to explain the plasma discharge [24–30]. The first model, known as dielectric breakdown model, was proposed by Vijn [24] and Ikonnopisov [30], which considered the discharge as local avalanche breakdown of the oxide layer. According to this model, the polarizing voltage should be linear with the thickness of the oxide layer in order to

maintain a sufficient electric field required for dielectric breakdown. However, the voltage increase became much slower after the ignition of discharges. Later, Yerokhin et al. [26] and Wang et al. [25] proposed the contact glow discharge electrolysis model. They suggested that free electrons generated from the electrolyte tended to inject into the gas envelope formed at the oxide–electrolyte interface, thus a glow discharge could be ignited in the gaseous media which results in the melting and quenching of the underlying oxide. The third model, named discharge-in-pore model, indicates that the plasma discharge was generated by discharge of gas in the coating–electrolyte interface or in the micropores of the coating, which might be induced by dielectric breakdown of a barrier layer in the bottom of the micropores [29]. This model was supported by the optical emission spectroscopy (OES) findings by several research groups [28,31] and the interconnected porous networks in the PEO coatings reported by Curran [27]. Although the initiation of plasma discharge is still controversial, a well-accepted coating growth mechanism on magnesium alloys has been proposed [32]. Firstly, a passive film formed on the substrate like the traditional anodizing, during which the voltage increased linearly. The growth and dissolution of the oxide film occurred simultaneously and competed, as shown in Figure 1a,b. At the critical point, localized dielectric breakdown occurred at the flaws of the oxide film and discharge initiated as demonstrated in Figure 1c. Materials at the nearest vicinity of the discharges were melted by the high temperature plasma and ejected to the coating surface through the discharge channel. After quenched by the cold electrolyte, a coating comprising complex compounds could be obtained as illustrated in Figure 1d. During the PEO process, different types of discharges could take place, as shown in Figure 1e. Discharges of types A and C occurred at the coating surface and the pores in the upper coating, which led to the incorporation of electrolyte species into the coating. Type B discharges took place at the oxide–metal interface, resulting in coating materials that contains substrate metal species as the main component. Obviously, type B discharges are much more intensive and might cause the structural defects such as holes, cracks, and connected porosity. In addition, type B discharges were responsible for the formation of pancake-like structure. This model successfully explained the three-layer structure of the PEO coatings as well as the pancake-like morphologies at the coating surface. It is generally accepted that PEO coatings on magnesium alloys have three-layer structures: the outer porous layer, the fairly compact middle layer and the compact but thin inner layer (typically less than 1 μm). Among them, the middle layer is responsible for good mechanical properties and corrosion resistance. A more detailed discussion about the phenomenon associated with the PEO process (acoustic emission, optical emission, time-voltage plot, etc.) as well as the effects of processing parameters (such as electrolyte composition, frequency, duty cycles) has exceeded the scope of this review, but can be found in review [33].

PEO coatings possess high wear and corrosion resistance, excellent thermal stability, and superior adhesion strength. However, despite these favorable properties, PEO coatings are inherently porous, containing numerous micropores and microcracks due to the intense discharging and gas evolution. These flaws can serve as diffusion paths for corrosive media, potentially compromising the long-term corrosion resistance of the coating [34]. Furthermore, PEO coatings typically exhibit high friction coefficient.

Therefore, it is crucial to regulate the mechanical, tribological, and anti-corrosion properties of PEO coatings. One way is to modulate the coating properties by modifying the PEO process itself. Such modification could include the electrical parameters (current mode, pulse frequency, duty cycle, current density, etc.) and the electrolyte compositions [35]. Organic additives are usually added into the electrolyte to alter the characteristics of micro-discharges. Suitable organic additives in specific electrolyte could effectively suppress the strong arcs which are destructive to the PEO coatings, thus optimized morphology and enhanced properties could be obtained [36]. Another effective method to improve the coating properties is to fabricate composite coatings with multifunction. Two common ways have been utilized to prepare PEO-based composite coatings: (1) in situ formation of composite coatings by adding functional particles in the electrolyte, and (2) post-treatments,

including sol-gel, organic coating, physical vapor deposition (PVD), and surface remelting. This review systematically summarizes the preparation and characterization of wear and corrosion-resistant PEO-based composite coatings on magnesium alloys, produced via in situ formation and post-treatments.

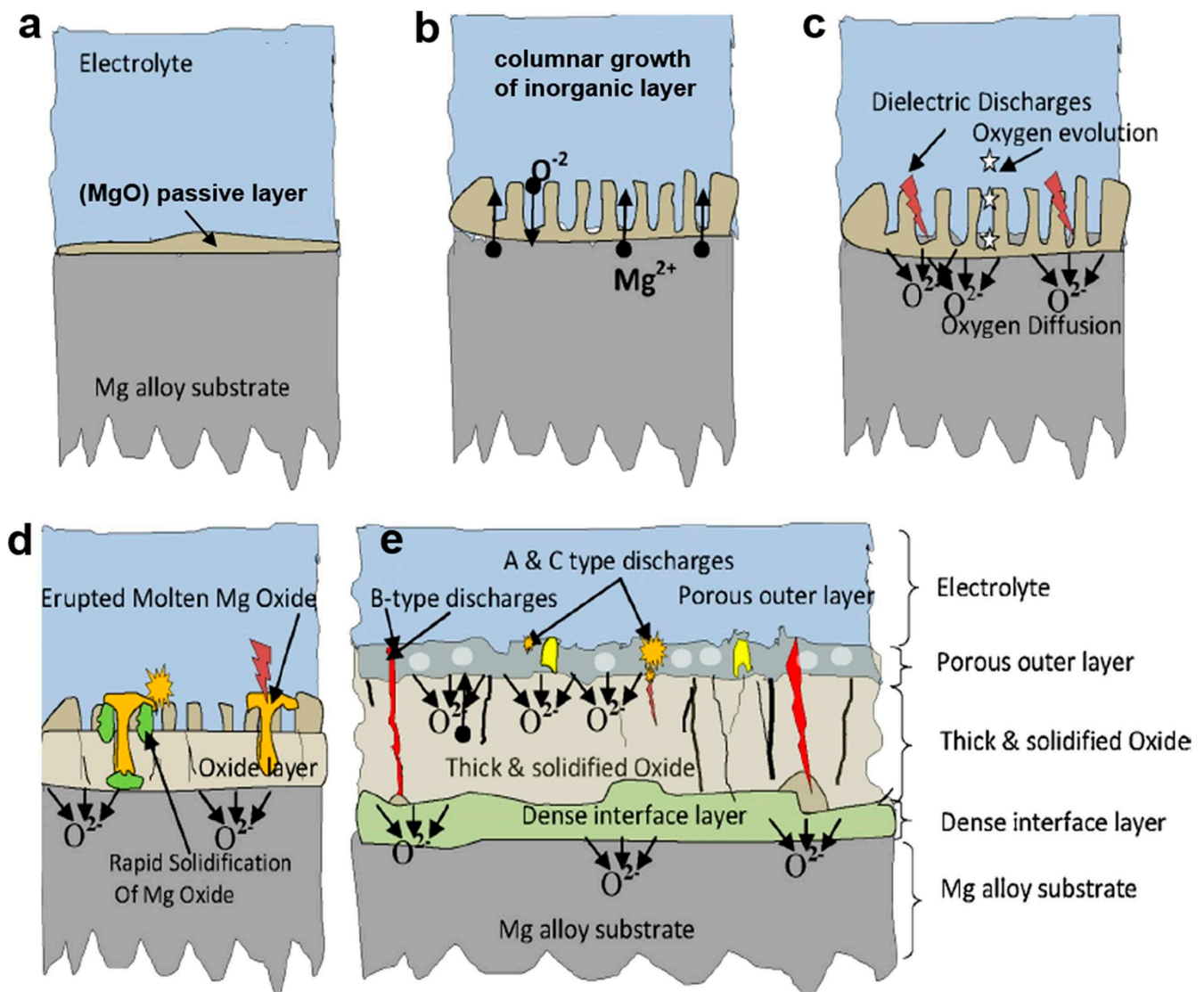


Figure 1. Schematic illustration of the growth process of PEO coating made on Mg alloy, (a) and (b) formation and growth of passive layer, (c) initiation of plasma discharge, (d) growth of PEO coatings and (e) formation of three-layered structure. (with permission from Ref. [32]; License number: 5574141493945, 2023, Elsevier).

2. Preparation and Characterization of PEO Composite Coatings on Magnesium Alloys

2.1. In Situ Formation of PEO Composite Coatings and Their Properties

The properties of PEO coatings are primarily influenced by their microstructures and phase compositions, which could be partially optimized by adjusting the electrical conditions such as voltage/current magnitude, mode, frequency, and duty cycle [37,38]. Nevertheless, it remains challenging to eliminate the high porosity inherent in PEO coatings and to control the coating composition. Modifying the electrolyte composition serves as an effective method to enhance coating properties. Particularly, the addition of particles into the electrolyte, which targets in situ incorporation of functional species or pore sealing in the PEO coatings, has gained significant attention [39,40]. In most studies, particles

are directly added as powder or sol, with external forces such as mechanical stirring, gas bubbling and ultrasonic agitation to prevent particle sedimentation and agglomeration. By adjusting electrical parameters, electrolyte composition, and properties of particles (size, melting temperature and chemical stability), either reactive or inert incorporation of particles into the coating could be achieved.

Adjusting electrical parameters can influence the energy of discharges, which in turn affects the incorporation mode of particles [41,42]. Particles with smaller sizes, lower melting points, and/or less chemical stability tend to be incorporated reactively. For instance, clay particles with low melting points undergo complete reactive incorporation into PEO coating on AM50 magnesium alloy [41,43,44]. With clay particle incorporation, amorphous PEO coatings with a composition similar to commercial bio-glasses can be obtained as the clay particles lower the sintering temperature and enhance the coating's glass formation ability [44]. Lu and co-workers reported that nanosized SiO₂ particles experience reactive incorporation while microparticles are inertly incorporated [45]. Particles with higher melting point are generally undergo inert incorporation and have a less effect on the phase composition of the PEO coatings.

Particle incorporation significantly influences the morphology and microstructure of PEO coatings. Liang et al. [46] prepared PEO coatings on AM60B magnesium alloy in alkaline phosphate electrolyte, with and without addition of TiO₂ sol. In the absence of titania sol, the coating reveals a rough surface appearance with relatively large pores and cracks, as shown in Figure 2a. The addition of titania sol into electrolyte results in a more uniform and compact surface with fewer structural flaws. As a result, the corrosion potential shifts to the positive direction significantly (about 114 mV) and the corrosion current density (4.338×10^{-8} A/cm²) decreases by more than three orders of magnitude compared to the uncoated magnesium alloy (5.2×10^{-5} A/cm²). These results show that the corrosion resistance of the magnesium alloy can be enhanced to a great extent by the oxide film formed in electrolyte with addition of titania sol. For the PEO coated Mg alloy AZ31, the hardness increased from 130 HV to 358 HV due to inertly incorporated Al₂O₃ nanoparticles [47]. Consequently, the wear track of coating with particle addition was much narrower and shallower in contrast to that of particle-free coating, as shown in Figure 3. In general, the addition of oxide particles to the electrolyte can reduce the number and/or size of the pores and improve the compactness of the coating, leading to significant improvements in wear and corrosion resistance. Several oxide particles have been introduced into the electrolyte to date, including Al₂O₃ [47–49], TiO₂ [46,50], SiO₂ [45,51], ZrO₂ [52], and CeO₂ [53–55]. However, there is no clear trend for the influence of particles' addition on the coating thickness. Researchers have reported that the composite coatings had similar thickness [52,53] or even became thinner with the addition of particles [45,54,56,57]. On the contrary, some reports also claimed that the coatings were slightly thicker in the presence of particles [47,58,59]. Most of the literature reported PEO composite coatings with a thickness of 10~40 μm, although coatings with thickness more than 100 μm could be obtained with optimized processing parameters [60].

The integration of both inorganic compounds and organic particles such as clay [44], 8-hydroxyquinoline [61], polytetrafluoroethylene (PTFE) [56], graphite [62], graphene [63], MoS₂ [64], WC [65], Si₃N₄ [66], TiN [67], SiC [60], LDH [68], and halloysite nanotubes [69,70] into PEO layers has been extensively explored. This approach has been revealed to mimic the advantageous effects of oxide particle incorporation, predominantly resulting in a reduction porosity and structural flaws within PEO coatings. Consequently, an enhancement in corrosion resistance is observed. In addition, the tribological performance of PEO coatings can be improved by the inclusion of particles exhibiting solid lubricating characteristics, namely PTFE, graphite, graphene oxide, and MoS₂. For instance, Guo et al. [56] illustrate this concept through producing a multifunctional PTFE-containing oxide composite coating on an AM60B magnesium alloy, which is achieved by using an alkaline phosphate electrolyte with addition of PTFE nanoparticles suspension. With the addition of PTFE in the electrolyte, a positive shift in the corrosion potential is observed,

accompanied by a decrease in the current density by an order of magnitude. In terms of friction coefficient, uncoated Mg, pure PEO coating, and PTFE-containing PEO coating display values of 0.2–0.4, 0.5–0.7, and 0.1–0.12, respectively. The superior corrosion and tribological performance of the PTFE-containing PEO coating could be attributed to a denser, more uniform surface alongside the non-sticking and solid lubrication properties of PTFE particles. Another study conducted by Zhao and co-workers incorporates graphene oxide (GO) into the electrolyte during the PEO coating process applied on AZ31 magnesium alloy [57]. The coated samples denoted as E0, E1, E2, and E3 are obtained in electrolyte containing 0, 1, 2, and 3 g/L GO, respectively. The pore area and band of the PEO coatings exhibit marked variations with different concentration of GO, as depicted in Figure 4. The E0 sample manifests the most extensive pore area and band, whereas the addition of GO into the electrolyte pronouncedly reduces the pore area and the width of the pore band. In particular, the E2 sample shows the smallest pore area and the narrowest pore band. Thus, the incorporation of GO during PEO processing can improve the microstructure compactness of the PEO coatings and reduce the porosity. Potentiodynamic polarization and electrochemical impedance spectroscopy (EIS) studies confirm that incorporation of GO substantially improves the corrosion resistance of PEO coatings. The superior corrosion resistance could be attributed to the barrier property of GO sheets which inhibit the permeation of aggressive electrolyte and increase the tortuosity for electrolyte diffusion pathway.

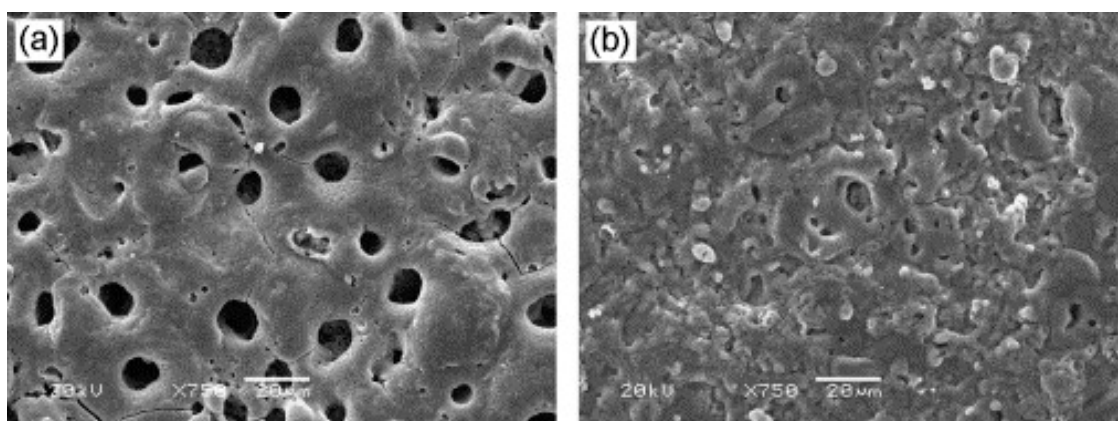


Figure 2. Surface morphologies of PEO coating formed on AM60B magnesium alloy formed in sodium phosphate (10 g/L) electrolyte (a) without and (b) with addition of 4 vol% titania sol. (With permission from Ref. [46]; License number: 5545700018632, 2023, Elsevier).

The recent trend towards developing protective coatings with active anticorrosion and self-healing capabilities, key attributes for enduring protection of metallic structures, has attracted the interest of numerous researchers [71]. These novel functionalities are primarily achieved through the encapsulation of corrosion inhibitors into “smart” nanocontainers. These nanocontainers have the potential to actively release corrosion inhibitors at corroded spots in response to external stimuli. Fortunately, such corrosion inhibitor loaded nanocontainers could be in situ incorporated into PEO coatings. Wu et al. [70] have demonstrate this approach using 2-aminobenzimidazole-loaded halloysite nanotubes (HNTs) as additives to the electrolyte for micro-arc oxidation of AZ31 magnesium alloys. According to their research, incorporation of halloysite nanotubes slightly increase the porosity and thickness of the PEO coatings, which should be attributed to a more powerful discharge process in electrolyte containing halloysite nanotubes. The EIS spectra of SEHi (PEO coating with 2-aminobenzimidazole loaded HNTs), SHE (PEO coating with HNTs), and SE (pure PEO coating) samples and bare substrate after immersion in 3.5 wt.% NaCl solution for varying durations are shown in Figure 5. SE sample has highest impedance during the first hour of immersion (Figure 5a), which might be related to the lowest porosity. However, after immersion for three hours (Figure 5c), the impedance of SEHi sample increases by more

than one order of magnitude and continues to rise. The 2-aminobenzimidazole released from HNTs facilitates the formation of stable passive layer, thereby inhibiting corrosion and boosting long-term corrosion protection. Such self-healing behavior has also been observed in other studies [68,69].

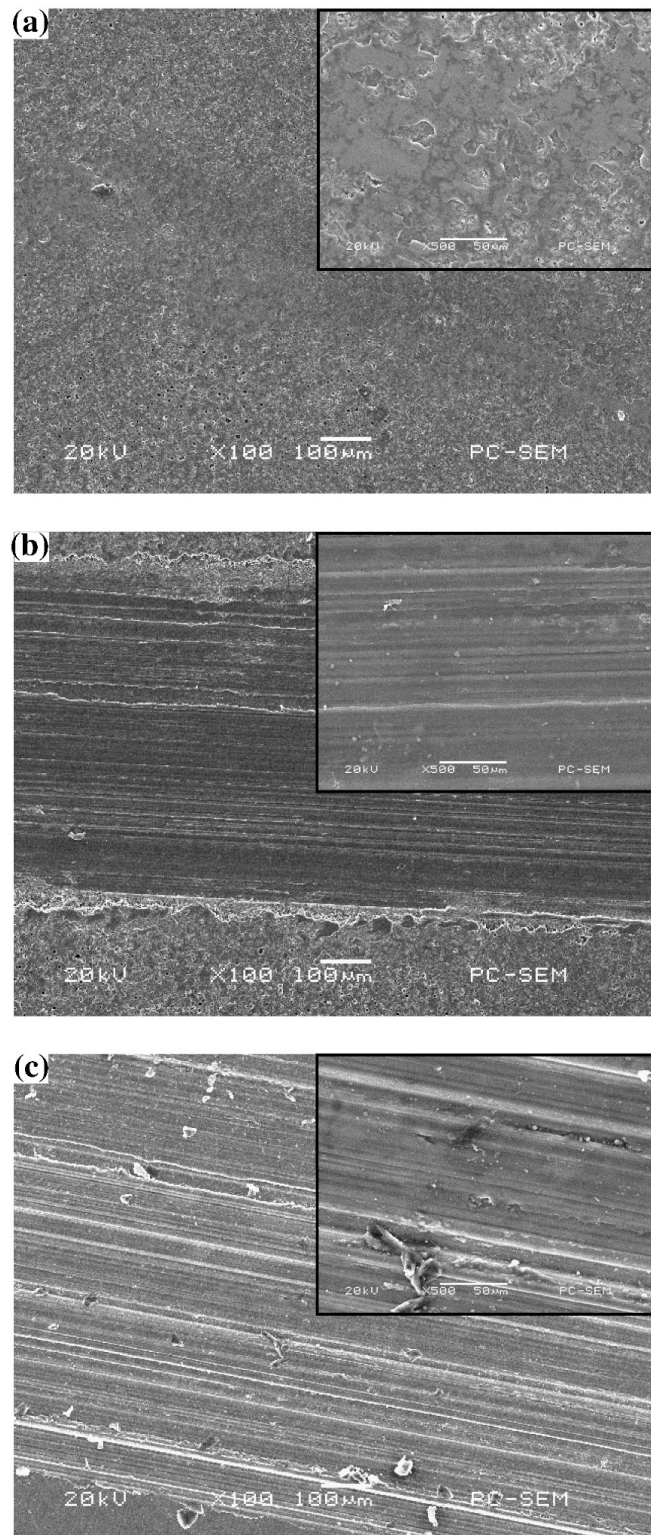


Figure 3. Wear track of (a) PEO coating with Al_2O_3 nanoparticles; (b) PEO coating without Al_2O_3 nanoparticles; (c) AZ31 substrate. (With permission from Ref. [47]; License number: 5545851211922, 2023, Elsevier).

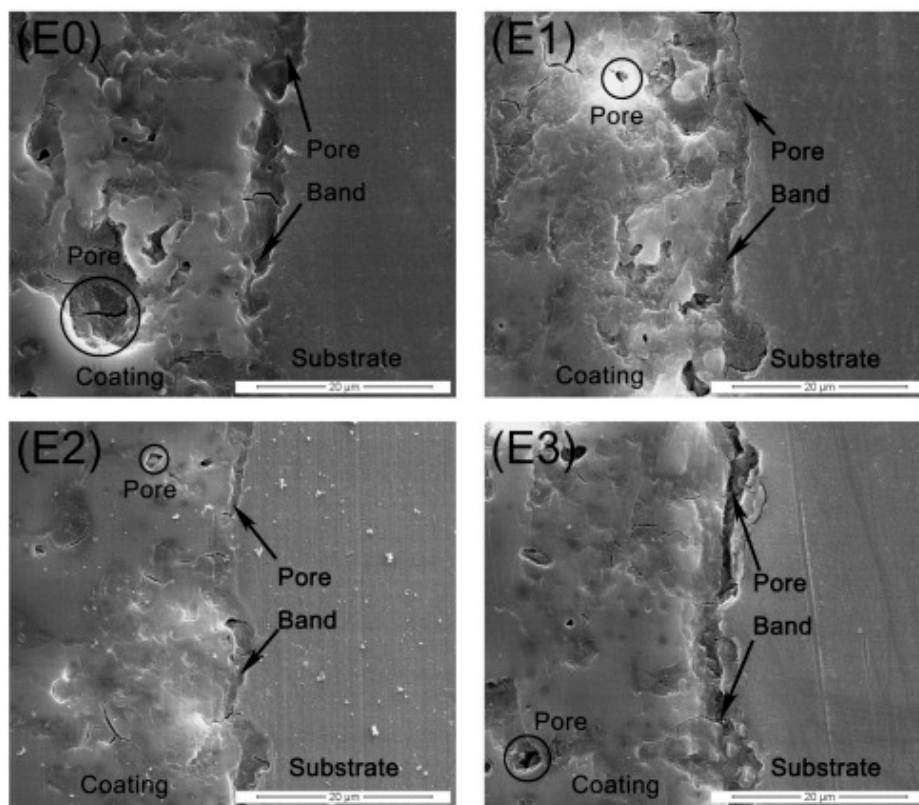


Figure 4. Cross-section morphologies of the PEO coatings prepared on AZ31 magnesium alloy in electrolyte with addition of GO. (With permission from Ref. [57]; License number: 5545830944037, 2023, Elsevier).

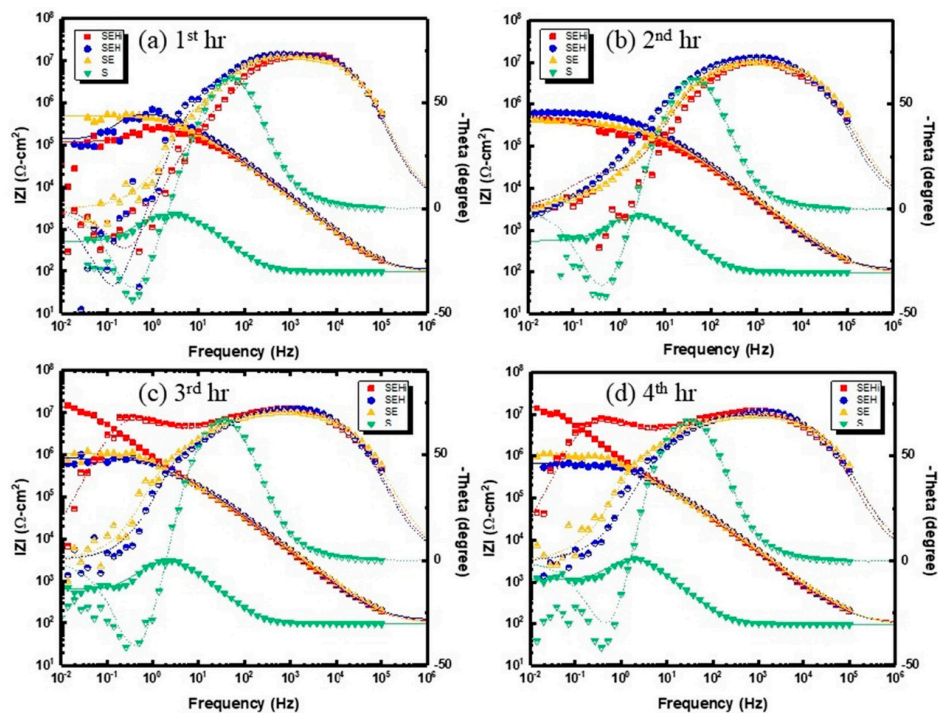


Figure 5. Evolution of EIS bode plot and bode phase-angle diagram of SEHi, SEH, SE, and AZ31 Mg substrate immersed in 3.5 wt% NaCl solution (a) first h, (b) second h, (c) third h, (d) fourth h. (With permission from Ref. [70]; License number: 5545850350678, 2023, Elsevier).

Importantly, there appears to be an optimal concentration of particles to be introduced into the electrolyte, above which the properties of prepared coatings deteriorate. Lou et al. [64] evaluate the influence of varying MoS₂ nanoparticle concentrations on the mechanical property and corrosion resistance of PEO composite coating on AZ31 magnesium alloy. The addition of 2.5 g/L MoS₂ nanoparticle into the electrolyte yields excellent adhesion, wear resistance, and the best corrosion resistance. However, adding more than 5 g/L MoS₂ nanoparticle to electrolyte impairs the mechanical properties of the coating because of the segregation of MoS₂ nanoparticles. Mashtalyar et al. [67] study the effect on TiN nanoparticles on the hardness and wear resistance of PEO coating prepared on MA8 magnesium alloys. The lowest porosity, highest hardness, and smallest wear rate are observed on coating prepared in electrolyte with addition of 3 g/L TiN nanoparticles. Table 1 summarizes particles which have been introduced to the PEO electrolyte and their effects on the tribological performance and corrosion resistance.

Table 1. Particles applied in PEO processing and their effects on coating's properties.

Particles	Substrate	Thickness without/with Particles (µm)	COF	Wear Rate	E _{corr} (V)	I _{corr} (µA/cm ²)	EIS Impedance (Ω·cm ²)	Ref.
0~30 g/L CeO ₂	AZ31	10/10	--	--	-1.45 vs. SCE	0.04	4 × 10 ⁶	[53]
5 vol.% ZrO ₂ sol	AZ91D	36/40	--	--	-1.216 vs. SCE	0.01436	--	[59]
5 g/L SiO ₂	AM50	45/25~33	0.66~0.72	4 × 10 ⁻⁴ mm ³ /Nm	-1.566 vs. Ag/AgCl	0.24	--	[45]
PTFE	AM60B	15/13	0.1~0.12	--	-1.557 vs. SCE	0.213	--	[56]
10 g/L Al ₂ O ₃	AZ31	15~17/16~20	0.35	--	-1.143 vs. SCE	0.3822	--	[47]
2 g/L CeO ₂	Pure Mg	--	--	--	-1.629 vs. SCE	0.187	3.57 × 10 ⁵	[55]
2.5 g/L MoS ₂	AZ31	13/20	--	0.9 × 10 ⁻⁶ m ³ /Nm	-0.13 vs. SCE	0.83	--	[64]
2 g/L SiC	AZ31	76~121/88~126	0.5~0.7	1~2 × 10 ⁻⁴ mm ³ /Nm	--	--	--	[60]
3 g/L TiN	MA8	20/19~21	0.5	19 × 10 ⁻⁶ mm ³ /Nm	--	--	--	[67]
2 g/L Si ₃ N ₄	AZ31	13/16~18	0.57	--	-0.19 vs. SCE	1.95	--	[66]
4 g/L WC	AZ31B	18.3/14.76	0.14	6.7 × 10 ⁻⁴ mg/Nm	--	--	--	[65]
10 g/L HNTs	AZ31	18~24/21~30	--	--	--	--	3.69 × 10 ⁷	[70]
LDH	AZ91	20.5/22.5	--	--	-1.51 vs. SCE	14.81	6.39 × 10 ⁴	[68]
2 g/L GO	AZ31	40.7/34.3	--	--	-1.44 vs. SCE	0.033	8.09 × 10 ⁵	[57]

2.2. Preparation of PEO Composite Coatings by Post-Treatments

Although addition of particles in electrolyte during PEO processing can reduce the porosity and improve the compactness of obtained coatings, the intrinsic porosity of the coating remains a concern. As a such, duplex/post-treatments are required to achieve enduring corrosion protection.

2.2.1. Laser Surface Remelting

Rapheal and coworkers [72] prepare hybrid coatings by PEO on MRI 230D magnesium alloy in silicate and phosphate electrolytes which are subsequently subjected to laser surface alloying (LSA) with Al and Al₂O₃. Pore-free hybrid coatings with hardness of 273 HV (Si-PEO+LSA) and 230 HV (P-PEO+LSA) are obtained, while a few solidification cracks are found. Both the PEO coatings exhibit friction coefficients of approximately 0.8, while hybrid coatings present values of around 0.5 against the AISI 52100 steel ball. Another study on pure Ti [73] demonstrates a 75% reduction in porosity on surface and cross-sectional area in hybrid coatings of laser treated PEO (L-PEO) compared to PEO coatings, achieved through carefully controlling the laser melting process. To date, only few papers have been

published on duplex treatment combining PEO processes and laser surface treatments, indicating a need for further research.

2.2.2. Vapor Deposition

Liang et al. [74] develop MAO/Ti-DLC hybrid coatings on AM60B magnesium alloys through a combination of MAO and filtered cathode arc deposition. The MAO monolayer exhibits a very high friction coefficient around 0.7–0.8; the Ti doped DLC monolayer fails after 350 s sliding test. In contrast, the MAO/Ti-DLC hybrid coating demonstrates superior tribological behavior with a stable friction coefficient below 0.2. The wear track depth is also significantly reduced. Yang et al. [75] deposit a Ti and N co-doped diamond-like carbon ((Ti:N)-DLC) film on MAO coated AZ80 magnesium alloys using a hybrid beam deposition system. The system consists of a DC magnetron sputtering of Ti target and a linear ion source (LIS) with C_2H_2 and N_2 precursor gas. The corrosion current densities are 5.159×10^{-5} , 2.002×10^{-6} , and 5.508×10^{-9} A/cm² for the magnesium substrate, MAO monolayer, and (Ti:N)-DLC/MAO hybrid coating, respectively. The friction coefficient decreases from 0.5 for MAO monolayer to 0.1 for (Ti:N)-DLC/MAO hybrid coating, as shown in Figure 6. Ning et al. [76] studied the effect of doping elements (H, Si and Cr) on the tribological and electrochemical properties of MAO/DLC hybrid coatings deposited on AZ31B magnesium alloy. They claim that H doping leads to lowest corrosion current density while Si doping provides the lowest friction coefficient. All MAO/DLC hybrid coatings show much lower wear rate ($3\text{--}4 \times 10^{-6}$ mm³/Nm) compared with that of MAO monolayer (10.5×10^{-6} mm³/Nm). Sun et al. [77] investigate the influence of PECVD post-treatment on the corrosion property of PEO coatings deposited on pure magnesium. Tetraethyl orthosilicate (TEOS), hexamethyldisiloxane (HMDSO), and tetramethyl orthosilicate (TMOS) are used as precursors. While pore-sealing effects are observed with HMDSO and TMOS precursors, the PECVD process cause obvious damage to the PEO coating. The competition between these two effects makes the influence of post-treatment on the corrosion property complicated. Only HMDSO precursor could effectively improve the corrosion resistance of the PEO coating.

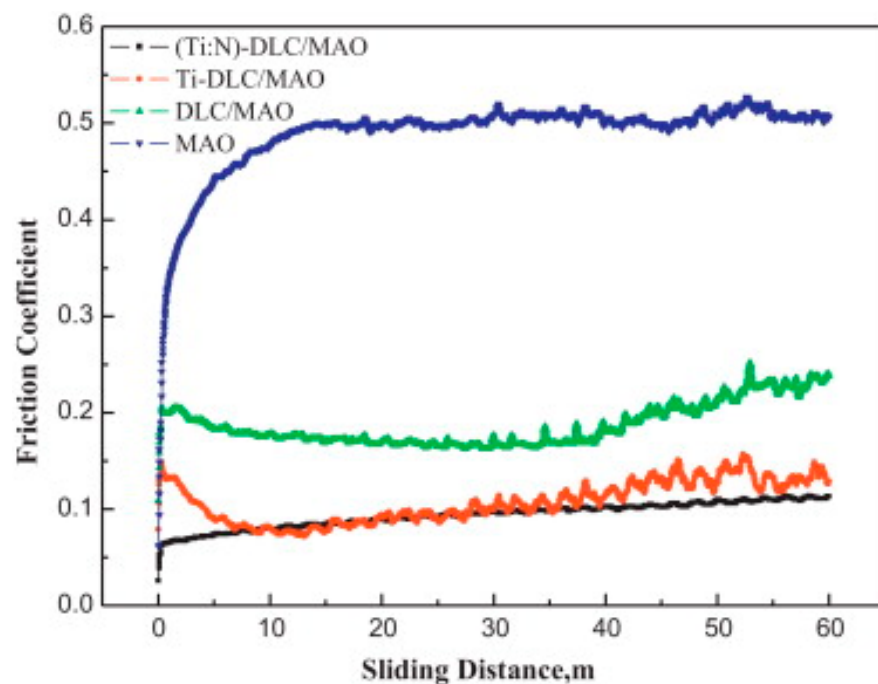


Figure 6. Coefficient of friction (COF) of the films coating AZ80 as a function of sliding distance. (With permission from Ref. [75]; License Number: 5546290720309, 2023, Elsevier).

2.2.3. Electroless Plating

Using Electroless plating (EP) to modify PEO coatings on magnesium alloys has attracted significant research interest. Among the plating materials, electroless nickel plating has high hardness, superior wear, and corrosion resistance, and has been extensively researched. However, direct electroless nickel plating on magnesium alloys is difficult because magnesium is extremely susceptible to galvanic corrosion. Thereby, only a few papers have been published [78,79]. Liu et al. [80] combine PEO coating with electroless nickel plating to protect AZ91 magnesium alloy. Compared with magnesium alloy substrate, PEO coating provides more uniform nucleation with higher density for EP processing. As a result, a high-quality EP layer forms on the top of PEO film. In addition, the high nucleation density provides more effective fastening sites between the EP top coat and the PEO intermediate layer, which is beneficial for adhesion strength. Zeng et al. [81] prepare a double-layer coating on AZ91D magnesium alloy by PEO followed with EP. The electroless plated Ni-P layer grows from the pores of the PEO film and a defect-free top coat is obtained. The open circuit potential of the double-layer coated AZ91D alloy (-0.3948 V) is significantly higher than that of the bare alloy (-1.5763 V). The corrosion current density decreases from 1.1185×10^{-4} A/cm² to 3.0904×10^{-6} A/cm². There are no noticeable corrosion pits on the surface of double-layer coated AZ91D alloy until 192 h neutral salt spray testing, indicating good long-term corrosion resistance. A similar result has been reported in another research using TiB₂ as a catalyst for the nucleation of nickel plating [82]. However, galvanic corrosion between magnesium alloy and nickel remains a concern in application of such double-layer coatings. Guo et al. [83] build a three-layer composite coating on AZ31B magnesium alloy which consists of the PEO film as bottom layer, the self-assembled nanoparticles (SANP) film as the intermediate layer and the EP plating as the top layer. The application of SANP film on PEO film forms a coherent bilayer, which provided effective protection for Mg alloy against galvanic corrosion and long-term immersion corrosion when combined with the compact EP plating. Table 2 summarizes the properties of composite coatings prepared by vapor deposition and electroless plating, which usually has high surface hardness.

Table 2. Properties of composite coatings prepared by PEO combined with vapor deposition and electroless deposition.

Top Coat	Substrate	COF	Wear Rate	E _{corr} (V)	I _{corr} (μA/cm ²)	EIS Impedance (Ω·cm ²)	Ref
Silicone	Pure Mg	--	--	-1.69 vs. SCE	0.003	1.32×10^7	[77]
Si-DLC	AZ31B	0.17	3.4×10^{-6} mm ³ /Nm	-1.347 vs. SCE	5.26	--	[76]
H-DLC	AZ31B	0.23	4.3×10^{-6} mm ³ /Nm	-1.484 vs. SCE	0.326	--	[76]
Cr-DLC	AZ31B	0.26	3.5×10^{-6} mm ³ /Nm	-0.1298 vs. SCE	85.2	--	[76]
Ti-DLC	AM60B	0.2	--	--	--	--	[74]
(Ti:N)-DLC	AZ80	0.1	--	-1.251 vs. SCE	0.0055	--	[75]
Ni-P	AZ91D	--	--	-0.3948 vs. SCE	3.09	1.103×10^4	[81]
SANP+Ni-P	AZ31	--	--	-0.42 vs. SCE	0.258	6×10^4	[83]

2.2.4. Electrodeposition and Electrophoretic Deposition

Electrodeposition, or electrophoretic deposition, is another widely employed post-treatment for PEO coatings. The intrinsic porosity of PEO coatings provides abundant loading sites for particles or deposits. The bonding strength of the top coat could be significantly enhanced by larger contact areas and interlock along rough interface between the MAO layer and top coat. Like the addition of particles in PEO electrolyte, various kinds of particles could be introduced into the solution for electrodeposition or electrophoretic

deposition, which offers numerous possibilities to modulate the coating properties [84–94]. Kannan et al. [84] modify the surface of pure magnesium by PEO processing followed with electrochemical deposition of calcium phosphate (CaP) and a double-layer coating is formed. In vitro electrochemical degradation tests in simulated body fluid (SBF) reveal that the PEO-CaP hybrid coating has much higher corrosion resistance. The corrosion current density of the PEO-CaP coated sample is ~99% and ~97% lower than that of bare magnesium and the PEO-only coated sample. In another research, Han et al. [85] claim that cathodic electrodeposition of the mixture of calcium hydrogen phosphate dihydrate (DCPD) and hydroxyapatite (HA) on the surface of PEO coated magnesium offers excellent corrosion resistance and biodegradability in SBF. Wang et al. [86] build a micro-arc oxidation/graphene oxide/stearic acid (MAO/GO/SA) superhydrophobic composite coating on AZ91D magnesium alloy by combining the MAO, electrodeposition, and self-assembly techniques. The electrodeposited GO has a typical laminar structure which can effectively close the pores of MAO coating. After being modified by SA, superhydrophobicity with a contact angle of 159.53° was obtained. Both the MAO/GO coating and the MAO/GO/SA composite coating had lower corrosion current density compared with the Mg alloy substrate and the MAO coating. The MAO/GO coating and the MAO/GO/SA composite coating were reduced by two and three orders of magnitude, respectively. Besides inorganic particles, electrophoretic deposition of organic polymers on the surface of PEO coating has also been studied [89–91]. Gnednikov et al. [89] develop a PTFE/PEO composite coating on MA8 magnesium alloy by using PEO and electrophoretic deposition. The electrophoretic deposition is conducted in the water suspension of superdispersed PTFE at 200 V. After curing at 315°C for 15 min, a compact PTFE layer is formed on the top of PEO film. As shown in Figure 7, The composite coating formed by electrophoretic deposition in electrolyte containing 20 g/L PTFE for 75 s shows the lowest corrosion current density of $1 \times 10^{-10} \text{ A/cm}^2$, which is three orders lower than that of PEO monolayer ($1.1 \times 10^{-10} \text{ A/cm}^2$). The friction coefficient as low as 0.05 could be obtained, as shown in Figure 8. The wear rate ($1.2 \times 10^{-6} \text{ mm}^3/\text{Nm}$) is also much lower than that of PEO monolayer ($4.1 \times 10^{-5} \text{ mm}^3/\text{Nm}$).

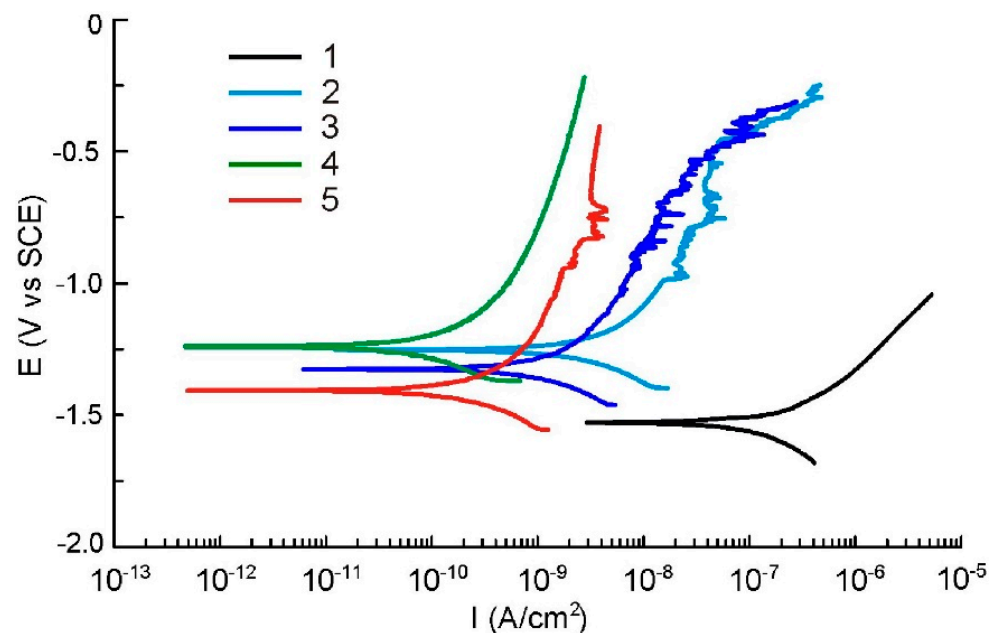


Figure 7. Polarization curves for the samples with base PEO coating (1) and composite coatings obtained at different process times: 25 s (2), 50 s (3), 75 s (4), and 100 s (5). Composite coating was formed in the electrolyte contained 20 g/L of SPTFE. (With permission from Ref. [89]; License Number: 5546480219082, 2023, Elsevier).

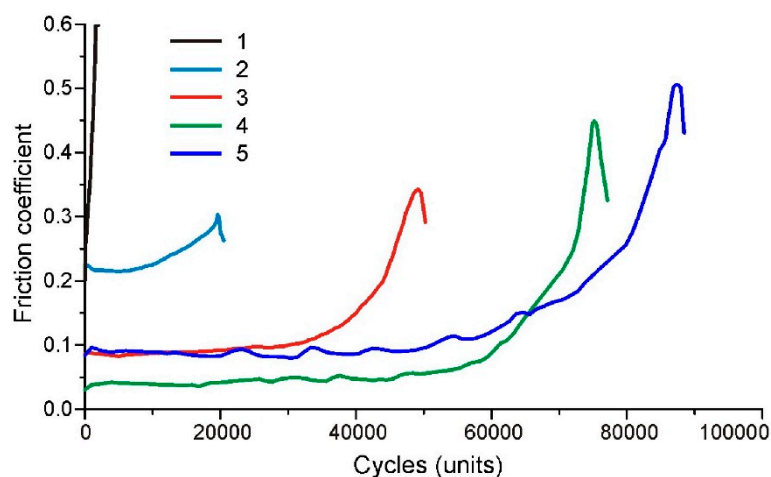


Figure 8. Dependence of the friction coefficient of the pair corundum ball/coating for the samples of MA8 magnesium alloys with PEO coating (1) and with composite coatings obtained at different electrophoresis times: 15 (2), 25 (3), 50 (4), and 75 (5) s. Composite coating was formed in the electrolyte contained 30 g/l of SPTFE. (With permission from Ref. [89]; License Number: 5546480219082, 2023, Elsevier).

Wang et al. [91] conduct electrophoretic deposition of MAO coated AZ31B magnesium alloy in a cathodic PPG(ED7000P) E-coat bath solution (70–78 wt.% deionized water, 17–25 wt.% epoxy resin, 3.2 wt.% titanium dioxide, and 1.8 wt.% aluminum silicate) at voltage 225 V for 2 min. After curing in the oven at 170 °C for 30 min, a smooth and pore-free top coat is formed. The open pores on the surface of MAO layer were fully filled with the epoxy top coat, which tightly adhered to the MAO layer. The bonding strength is significantly enhanced by interlocking along the rough interface and larger contact areas between the MAO layer and top coat. The corrosion current decreased from 1.89×10^{-6} A/cm² for MAO coating to 1.93×10^{-8} A/cm² for MAO-Epoxy hybrid coating.

2.2.5. Sol-Gel

Sol-gel, which is known as a simple, environmentally friendly, and inexpensive process, has been used for modification of PEO coatings on magnesium alloys [34,95–105]. Shang et al. [95] synthesize SiO₂-ZrO₂ sol by hydrolysis of ethyl silicate and zirconyl chloride octahydrate. The sol is applied to the MAO coating on AZ91D magnesium by dipping and then cured at 150 °C for 1 h. The sol-gel layer effectively seals the pores and microcracks in the MAO coating. As a result, the corrosion potential of the composite coating increased by 920 mV and the corrosion current density decreased by two orders when compared with the MAO monolayer. Shi et al. [104] prepare the MAO-TiO₂ composite coating on pure magnesium by combining MAO and sol-gel. An improved anti-corrosion behavior was observed in Hanks' solution at 37 °C. Guo et al. [97,98] synthesize sol of self-assembled nanophase particles (SANP) through hydrolysis of 3-glycidoxypropyltrimethoxysilane (GPTMS) and tetraethoxysilane (TEOS) in de-ionized water followed with crosslinking by tetramine (TETA). Then the SANP sol is applied to the MAO coating on AZ31B magnesium alloy and a bilayer composite coating is formed. The bilayer composite coating could effectively protect AZ31B magnesium alloy in 0.005 M NaCl solution for more than 354 h. In another study conducted by Merino et al. [100], the epoxide ring-opening reaction of GPTMS is initiated by 1-Methylimidazole (MI) instead of TETA. As a result, organic-inorganic hybrid coatings with high crosslinking characteristics are obtained. Li et al. [96] combine the PEO technique and sol-gel method for corrosion protection of magnesium-lithium alloy. Immersion tests in 3.5 wt.% NaCl solution demonstrate that the composite coatings can protect magnesium-lithium alloys for more than 800 h. More recently, several improvements have been introduced to the traditional sol-gel method. For instance, Li et al. synthesize the UV curable ZrO₂ sol by using acetylacetone as chelating agent [99]. Then the

sol is applied on MAO coating of AZ91D magnesium alloy. As shown in Figure 9, compared with the sol-gel layer cured at high temperature which typically has numerous cracks, the UV cured sol-gel layer is denser without cracks and provides better corrosion resistance.

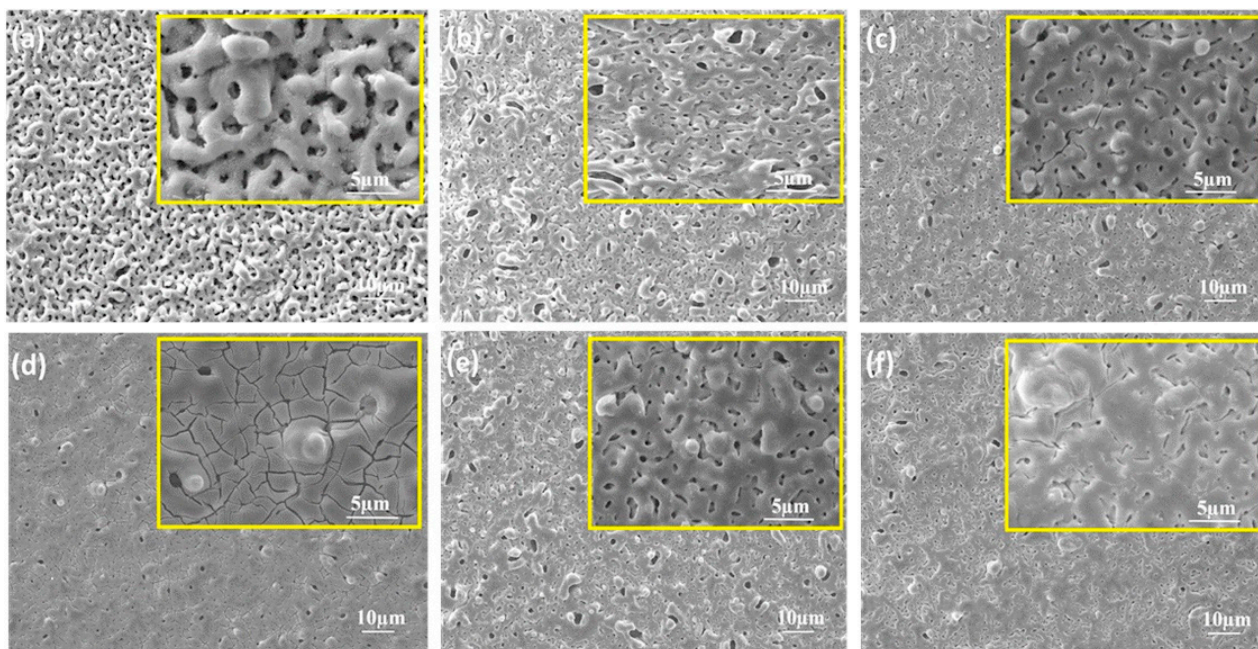


Figure 9. Surface morphologies of different coatings: (a) the MAO coating; (b–d) are the ZrO_2/MAO composite coatings heat treated at 100 °C, 275 °C and 425 °C, respectively; (e,f) are the surface morphologies of ZrO_2/MAO composite coatings irradiated by UV light for 1 h and 2 h, respectively. During the UV irradiation, the temperature is controlled at 100 °C. (With permission from Ref. [99]; License number: 5546941262738, 2023, Elsevier).

Li et al. [103] develop a hydrophobic coating on AZ91 magnesium alloy by PEO followed by two-step sol-gel treatment. The PEO coated sample is soaked by the silica sol and then modified with hexadecyltrimethoxysilane (HDTMS). The two-step hydrophobic coating provides better corrosion resistance with the corrosion current density decreasing from 10^{-5} to 10^{-7} A/cm². Additionally, no significant changes were observed on the surfaces of the treated samples after 30 days of immersion in NaCl solution, as shown in Figure 10. In another research conducted by Qiu and co-workers [106], magnetic Fe_3O_4 nanoparticles are modified with HDTMS and then dispersed in dopamine solution. The sol-gel layer is applied to the PEO coating on ZK60 magnesium alloy under magnetic field. A superhydrophobic surface with a water contact angles as high as 157° is formed. The corrosion current density of the superhydrophobic film was decreased to 14.39 nA/cm² compared with the bare sample, 0.105 mA/cm², in 3.5 wt.% NaCl solution.

Chen et al. introduce three different corrosion inhibitors (sodium salts of glycolic, 4-aminosalicylic and 2,6-pyridinedicarboxylic acids) into PEO/Sol-gel hybrid coatings on AZ91 magnesium alloy. Localized electrochemical technique (scanning vibrating electrode technique, SVET) is used to reveal the active corrosion protection provided by the corrosion inhibitors. As shown in Figure 11, most of the inhibitors demonstrate strong inhibiting effect after several hours of exposure. The corrosion activity of inhibitor-containing samples is suppressed to much lower values by 24 and 48 h of immersion. Similar results are reported by Galio [107] using 8-Hydroxyquinoline and Ivanou [105] using 1,2,4-triazole as corrosion inhibitors.

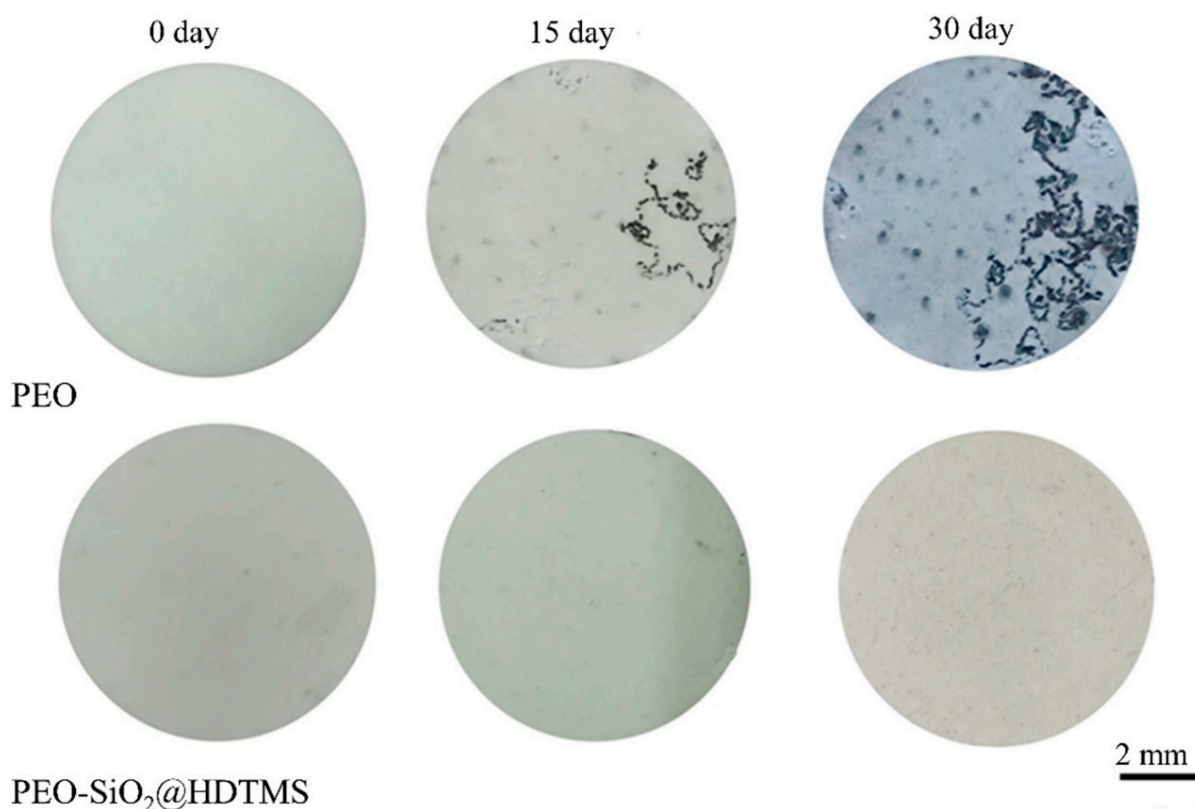


Figure 10. Optical morphology of PEO and PEO-SiO₂@HDTMS samples after the immersion test for 15 and 30 days. (With permission from Ref. [103]; License number: 5546951109080, 2023, Elsevier).

2.2.6. Hydrothermal Treatment

As a simple and cost-effective way to deposit protective coatings on metallic surface, hydrothermal treatment could also be applied to PEO coated magnesium alloys [108–123]. The most frequently used materials to seal the pores of PEO coatings on magnesium alloys are calcium phosphate, magnesium hydroxides (CaP), and layered double hydroxides (LDHs), although other compounds are also reported [115,116]. For instance, Chang et al. [108] prepare the Ca and P incorporated MAO coating on AZ31 magnesium alloy in electrolyte containing Na₂HPO₄ and EDTA-Ca. Ca and P exist in the MAO layer as amorphous phase. After being hydrothermally treated in deionized water, dicalcium phosphate dihydrate (DCPD) crystals form on the coating surface and seal the pores. The corrosion resistance of hydrothermally treated coating in Hank's solution increased and pitting corrosion disappeared. In the research conducted by Yao and coworkers [109], Ca is introduced to the composite coating during the hydrothermal process. Based on their study, pH of the hydrothermal solution affects the morphology and composition of the hydrothermal layer, as shown in Figure 12. At pH 5.6, the hydrothermal layer is flake-shaped, with the main crystalline of DCPD and hydroxyapatite (HA). At pH 9.4, the hydrothermal layer is rod-shaped with the main crystalline of HA. The corrosion resistance of the composite coatings is one order of higher than MAO coating and two orders higher than Mg substrate, due to the excellent sealing effect. Toro et al. [115] carry out hydrothermal treatment on PEO coated AZ31B magnesium alloy in Na₂CO₃, NaAlO₂+NaF, and NaAlO₂ solutions, respectively. The NaAlO₂+NaF demonstrate best sealing behavior with formation of MgAl₂O₄ and MgF₂, and the best anti-corrosion behavior is observed in the natural salt spray test. Dou et al. [116] fabricate a dense Ca₃Al₂(OH)₁₂ layer on the PEO coating by hydrothermal process in a slurry containing Ca(NO₃)₂·4H₂O and Al(NO₃)₃·9H₂O, and the corrosion resistance is enhanced.

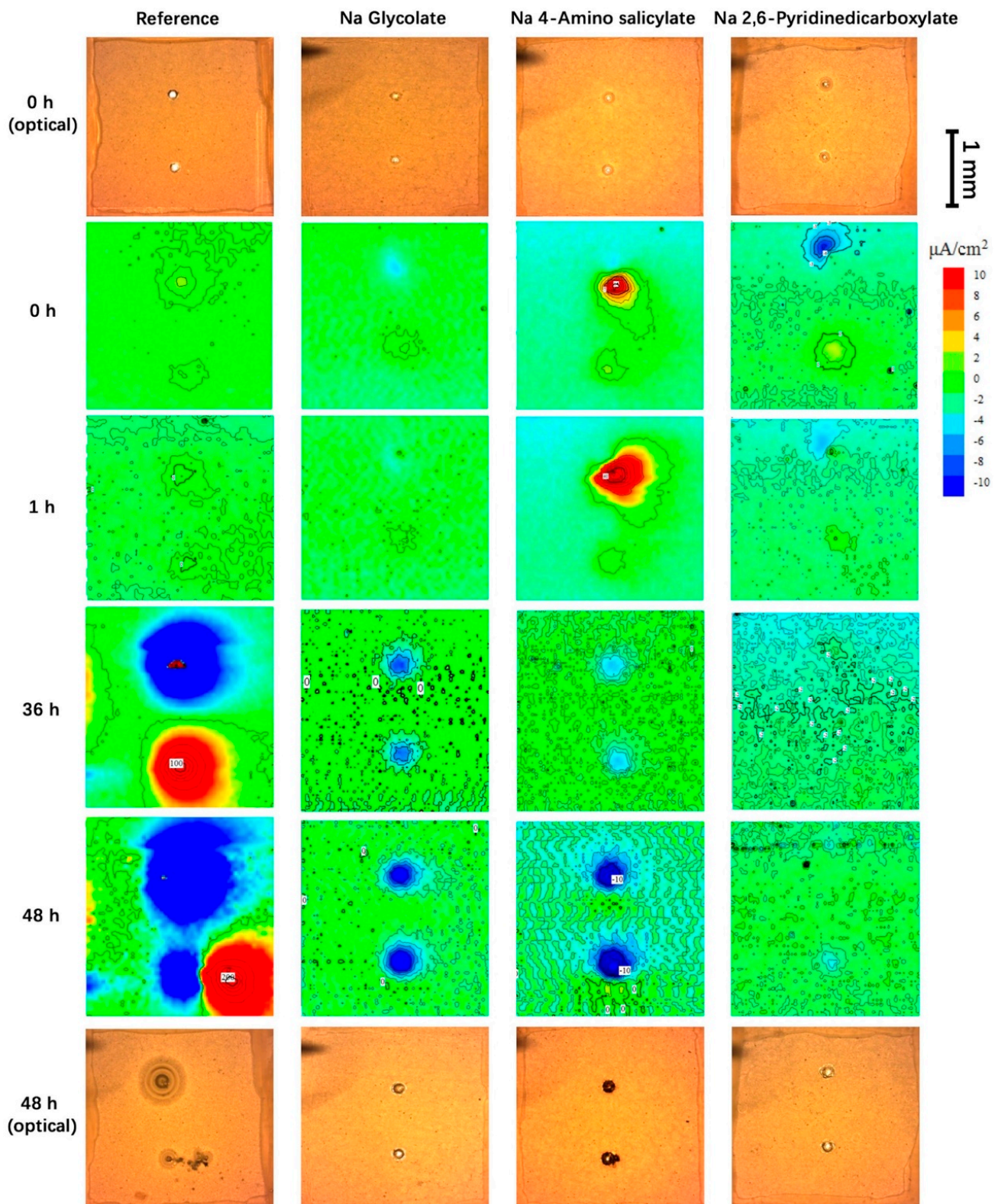


Figure 11. Optical images of the PEO-SG samples and SVET maps of current recorded above the surface of the PEO-SG samples. The time of exposure and inhibitors are indicated. (With permission from Ref. [71]; License number: 5546970628602, 2023, Elsevier).

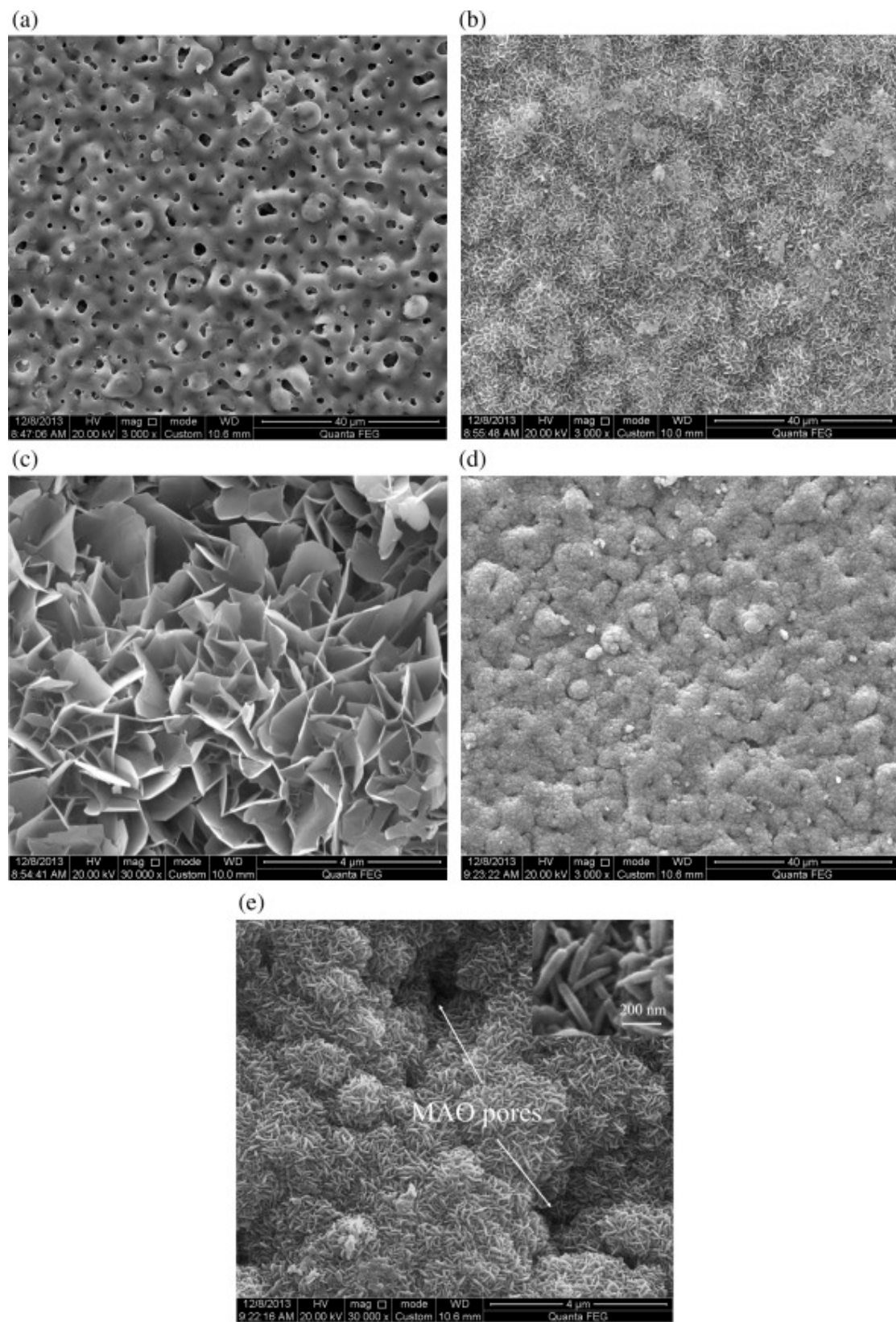


Figure 12. Surface morphologies of the MAO coating (a) and the compound coatings formed at pH 5.6 (b,c) and at pH 9.4 (d,e). (With permission from Ref. [109], License number: 5547041185186, 2023, Elsevier).

LDHs are made up of positively charged brucite-like layers and an interlayer region containing various anions and solvation molecules. Such a special structure of LDHs makes it a desirable nanocontainer for corrosion inhibitor. Zhang et al. [123] realize in situ LDHs growth on PEO coating formed AZ31 magnesium alloy in sodium aluminate electrolyte. The degradation of the anodic films and dissolution of the AZ31 substrate during the hydrothermal process provide internal sources of Mg^{2+} and Al^{3+} for LDHs growth. After hydrothermal treatment, the corrosion current density of the composite coating decreases by one order of magnitude. They also introduce Ce^{3+} into the aforementioned system and then modify it with phytic acid [124] for active corrosion protection, which is confirmed by SVET measurements. Wu et al. [121] synthesize in situ an Ag-Al LDHs film on the PEO coated AZ31 magnesium by hydrothermal process and then modify by stearic acid (SA), sodium laurate (SL), myristic acid (MA), and 1H, 1H, 2H, and 2H-perfluorodecyltrimethoxysilane (PFDTMS). Superhydrophobicity is obtained by modification of SA, SL, and MA, while the PFDTMS modification provides a static contact angle of 145.5° . Due to the high hydrophobicity and excellent sealing effect, the PFDTMS modified composite coating demonstrate best anti-corrosion behavior. No corrosion pit could be observed after 14 days immersion in 3.5 wt.% NaCl solution, as shown in Figure 13. The in situ LDHs growth on PEO coating prepared in phosphate and silicate electrolytes could be realized by addition of Al^{3+} cations into the hydrothermal solution [110]. The corrosion inhibitor could be loaded by in situ intercalation during the hydrothermal process [112,124,125] or by ion-exchange after the hydrothermal process [111,114,120]. For instance, Chen et al. load corrosion inhibitor 8-Hydroxyquinoline (8-HQ) on GO particles, then the 8-HQ@GO composites are dispersed in the hydrothermal solution. During hydrothermal treatment, the 8-HQ@GO composites are in situ doped into LDHs layer. The prepared MAO-LDHs/8-HQ@GO composite coating demonstrate excellent anti-corrosion and self-healing behavior. Inorganic corrosion inhibitors, such as PO_4^{3-} [114] and $V_2O_7^{4-}$ [111], could be intercalated into LDHs by ion exchange. Table 3 summarize some composite coating systems fabricated by PEO combined with electrophoretic deposition, sol-gel method, and hydrothermal treatment.

Table 3. Summary of composite coatings prepared by PEO combined with electrophoretic deposition and sol-gel method.

Top Coat	Substrate	Method	Achieved Functions	Ref
CaP	Pure Mg	PEO + Electrophoretic deposition	Improved biocompatibility and reduced degradation in SBF	[84]
HA + DCPD	Pure Mg	PEO + Electrophoretic deposition	Excellent corrosion resistance in SBF	[85]
GO + SA	AZ91D	PEO + Electrophoretic deposition	Superhydrophobic, excellent corrosion resistance	[86]
PTFE	MA8	PEO + Electrophoretic deposition	Excellent self-lubricating and wear resistance, good corrosion resistance	[89]
Epoxy resin	AZ31B	PEO + Electrophoretic deposition	Excellent bonding strength and corrosion resistance	[91]
GPTMS	AZ31B	PEO + Sol-gel	Excellent corrosion in immersion test	[100]
ZrO ₂	AZ91D	PEO + Sol-gel	UV curable at low temperature, denser structure	[99]
Corrosion inhibitors + SiO ₂ -TiO ₂	AZ91	PEO + Sol-gel	Active corrosion protection	[107]
DCPD	AZ31	PEO + hydrothermal	Eliminating pitting corrosion in Hank's solution	[108]
Ce ³⁺ & phytic acid modified LDHs	AZ31	PEO + hydrothermal	Active corrosion protection	[124]
LDHs modified with SA, AL, MA and PFDTMS	AZ31	PEO + hydrothermal	Superhydrophobic, excellent corrosion resistance	[121]
Corrosion inhibitors loaded LDHs	AZ31	PEO + hydrothermal	Active corrosion protection	[111,112,114,120]

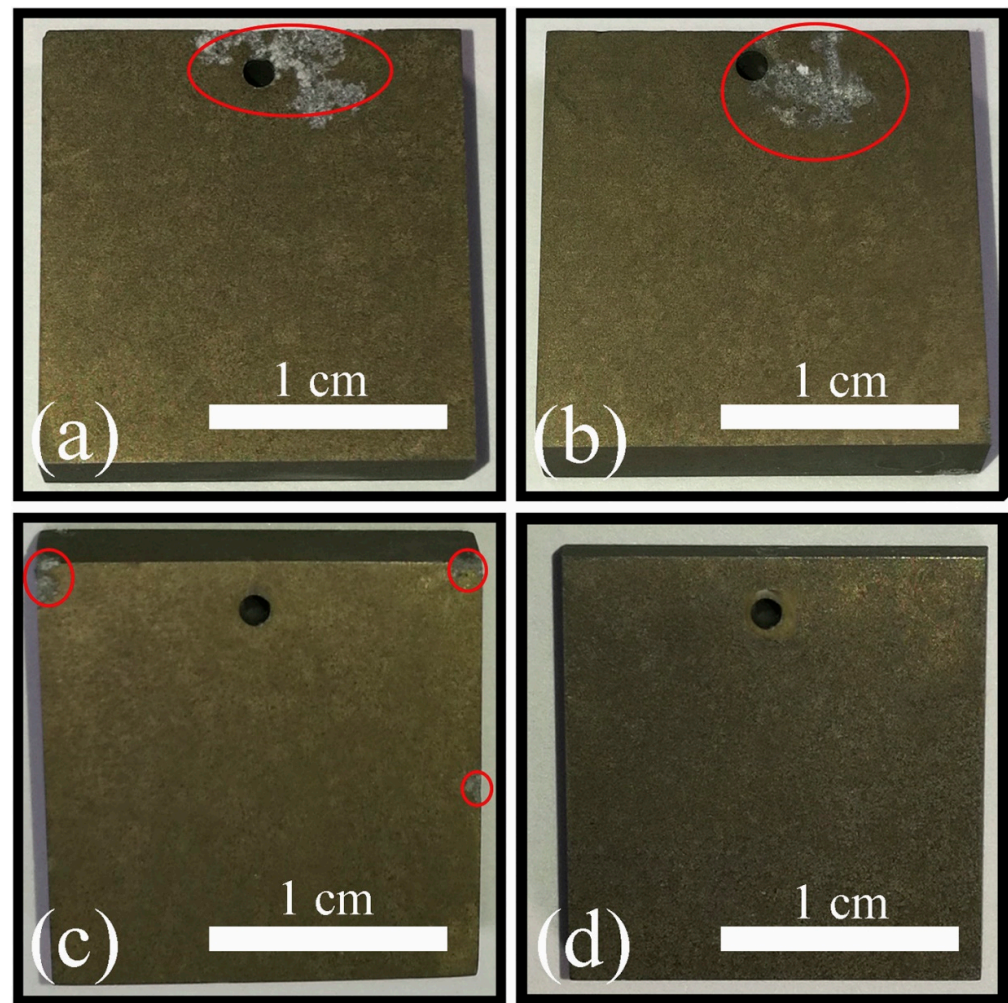


Figure 13. Photographs after immersion in 3.5 wt% NaCl solution for 14 days of the AZ31 specimens with films modified using: (a) SA; (b) SL; (c) MA; and (d) PFDTMS. (With permission from Ref. [121], license number: 5547050230526, 2023, Elsevier).

2.2.7. Organic Paint

Organic paint has been widely applied on the surface of metallic components to improve the corrosion and wear resistance. However, direct spraying of organic paint on magnesium alloys is doubtful due to the low bonding strength. On the other, PEO coating has superior adhesion strength with substrate due to its unique growth pattern. Therefore, many composite coatings have been developed for protection of Mg alloys, combining the advantages of PEO and organic paint [34,126–141]. Wang et al. [126] prepare a protective composite coating on AZ31B magnesium alloy by anodizing followed with immersion in maleic anhydride-g-liquid polybutadiene (MALPB) solution. MALPB, which has low molecular weight and low viscosity, infiltrate into the pores and cracks in the oxide layer so that a compact composite coating is formed. The composite coating provides better corrosion protection for AZ31B magnesium alloy against salt spray tests. Arrabal et al. [127] investigate the effects of PEO and fluortitanate-zirconate pre-treatment on mechanical and corrosion properties of a polyester-based polymer coating on AZ31 magnesium alloy. The PEO-polymer coating showed excellent adhesion and acceptable impact resistance, the latter being inferior to that of the Ti/Zr-polymer coating, which could be attributed to higher stiffness of the PEO coating. Additionally, the PEO-polymer composite coating provides a much more noticeable corrosion protection than Ti/Zr-polymer composite coating. Ivanou et al. [34] seal the PEO coated ZE41 magnesium alloy with a hybrid

epoxy-silane paint. After immersion in 0.6 M NaCl solution for 31 days, the impedance modulus at low frequency for the sealed samples remained more than $6 \times 10^9 \Omega \cdot \text{cm}^2$ without any indication of corrosion onset. Lu et al. [141] add pure magnesium particles into the commercial epoxy KFH-01 and then spray this Mg-rich primer on AZ91D magnesium alloys with and without MAO pre-treatment, respectively. With MAO pre-treatment, the adhesive strength of the Mg-rich primer on AZ91D alloy is significantly increased. After salt spray testing for 2400 h, the EIS spectra of the composite coating display a partial semi-circle, and the impedance modulus is higher than $10^{10} \Omega \cdot \text{cm}^2$ at a low frequency, indicating superior corrosion resistance behavior. Cui et al. [129] fabricate a polyurethane layer on the top of MAO coated AZ91D magnesium alloy. The composite coating provides excellent corrosion protection after immersion in a 3.5 wt.% NaCl aqueous solution for 168 h. In addition, the tribological behavior is enhanced and wear resistance is increased with polyurethane layer. Castellanos et al. [128] investigate the effects of sol-gel, PTFE, and acrylate-ethylene copolymer with nanoparticles on the corrosion and tribological behaviors of PEO coated AZ91D magnesium alloys. Although all post-treatments improve the corrosion resistance, only acrylate-ethylene copolymer has improved the tribological behavior and a friction coefficient as low as 0.15 could be obtained. Liu et al. [132] study the corrosion and tribocorrosion behaviors of MAO-based composite coating on AZ31 magnesium alloy, which has a top layer consists of polyamide-imide (PAI) and PTFE. The MAO coating is a hydrophilic surface with a contact angle of 55° , while the polymer coating exhibits a hydrophobic surface with a contact angle of 101° . The composite coating has excellent corrosion resistance with a corrosion current density of $6.68 \pm 1.1 \times 10^{-10} \text{ A/cm}^2$, which is three and five orders of magnitude lower than the MAO monolayer and AZ31 alloy substrate, respectively. The friction coefficient decreases from 0.4 (MAO monolayer) to <0.1 (MAO-PP composite coating) in 3.5 wt.% NaCl solution, as shown in Figure 14. Additionally, the wear volume loss is significantly decreased, particular under higher load, as shown in Figure 15.

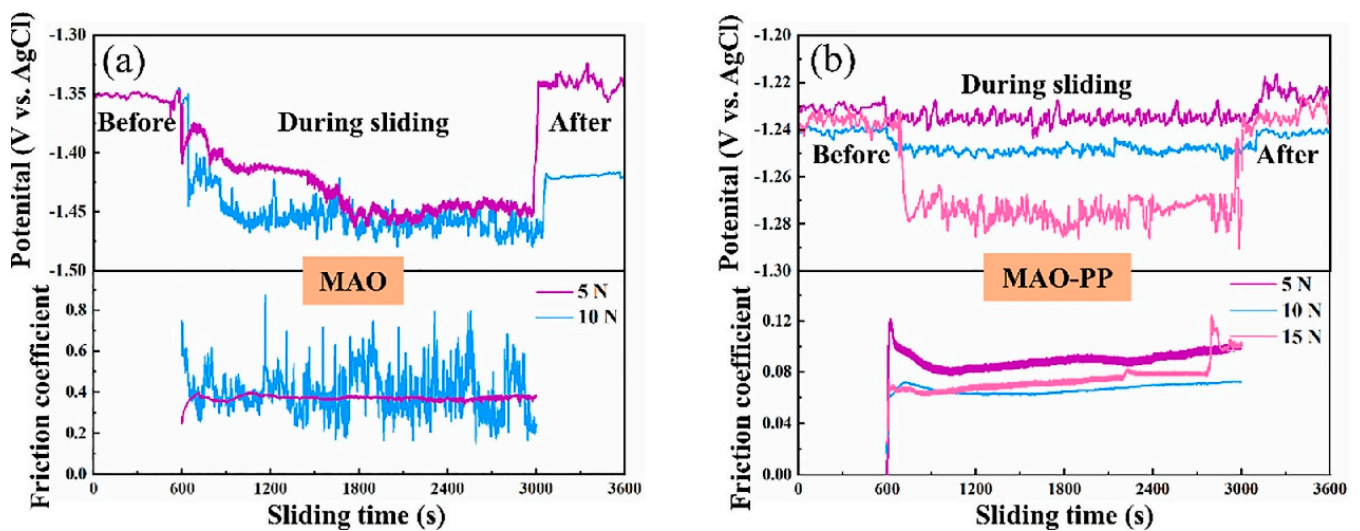


Figure 14. Variation in OCP with time recorded before, during, and after sliding under different loads in 3.5 wt.% NaCl solution with the COF values of MAO (a) and MAO-PP (b). (With permission from Ref. [132] under a Creative Commons license, Elsevier, open access).

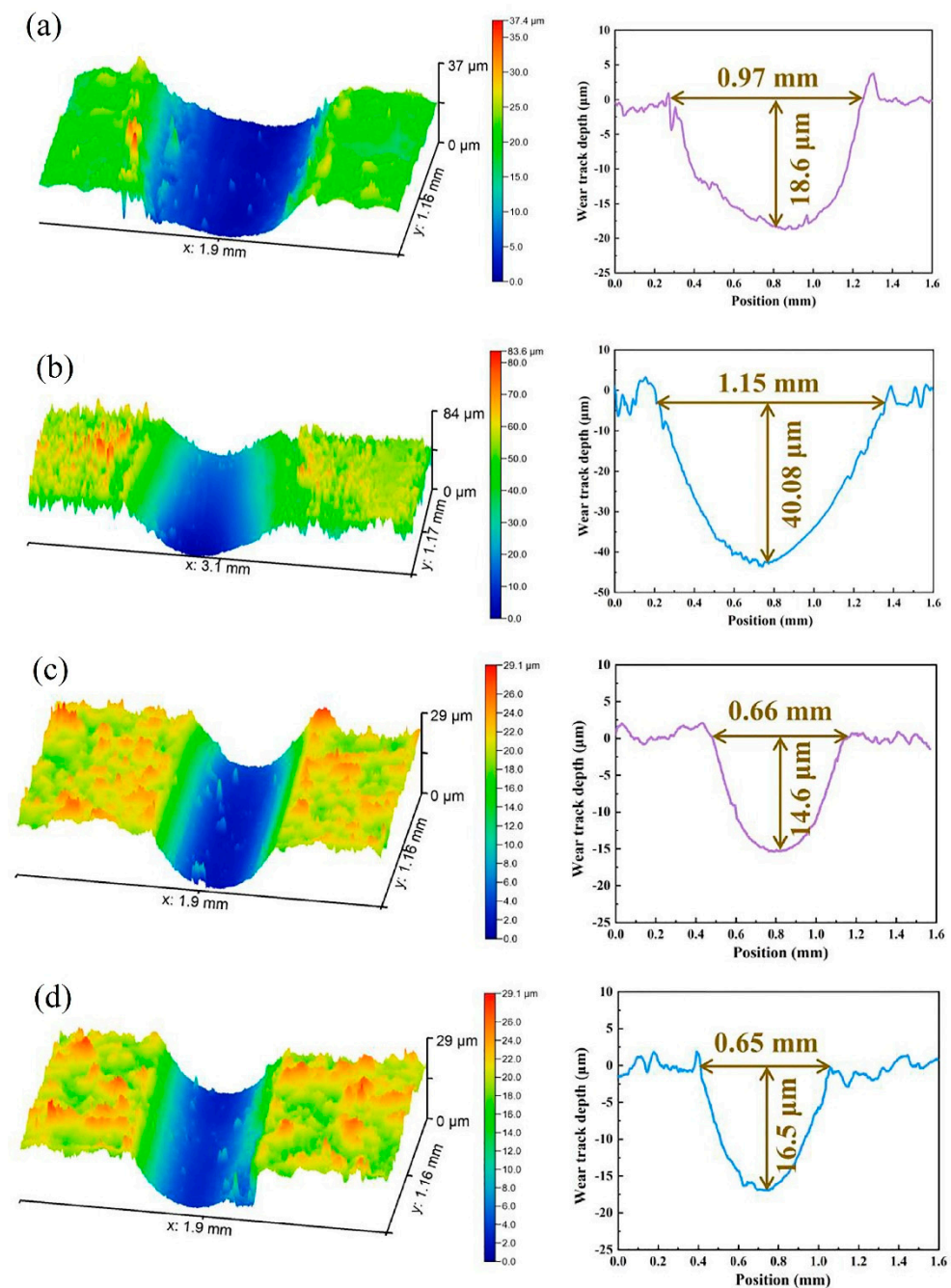


Figure 15. Three-dimensional morphologies of the wear tracks and cross-sections for (a) MAO sample under 5 N load, (b) MAO sample under 10 N load, (c) MAO-PP sample under 5 N load, and (d) MAO-PP sample under 10 N load after tribocorrosion. (With permission from Ref. [132] under a Creative Commons license, Elsevier, open access).

Recently, coatings with active corrosion protection have attracted great attention. Using corrosion inhibitors is a common way to realize active corrosion protection of metallic components. However, direct addition of corrosion inhibitors into polymer coating should be carefully controlled since the adding methods and the distribution of the inhibitors in the coating have great influence on the corrosion resistance and mechanical properties of the coatings. To address this concern, micro-/nano-containers are introduced in the coating system. For instance, Zhang et al. [133] coat the epoxy resin doped with Ce-loaded zeolite microparticles on PEO treated AZ31 magnesium alloy. The composite coating has a good self-healing ability against corrosion. Zhang et al. [140] study the influence of

positioning of nanocontainers in the MAO/epoxy composite coatings on the corrosion resistance. According to their research, when corrosion inhibitors-loaded mesoporous silica nanocontainers (MSN) are filtrated into the pores of MAO layer, the effectiveness of corrosion inhibitors is much higher, compared with MSN loaded within the epoxy layer. Therefore, a better self-healing behavior is observed, as shown in Figure 16. On the other hand, MSN loaded in epoxy layer could effectively reduce micropores and/or structural defects of the epoxy layer. As a result, higher impedance is obtained for the intact coating.

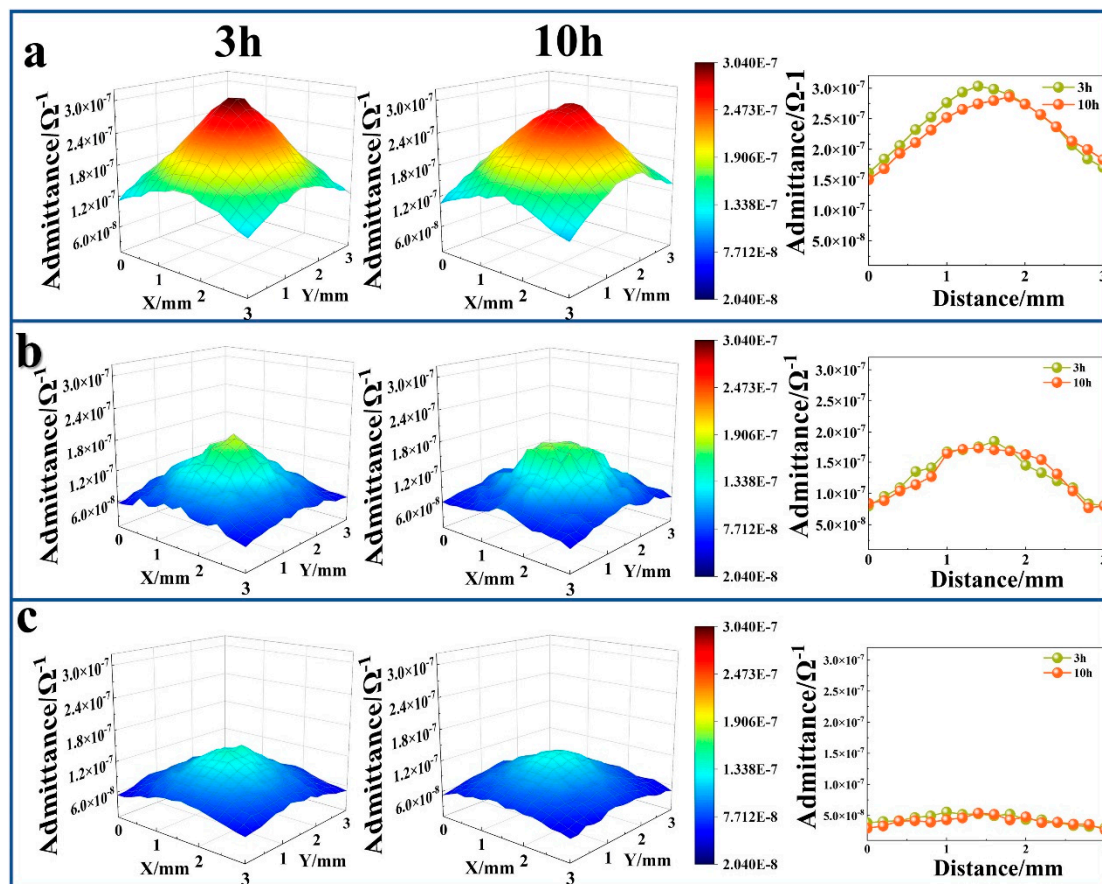


Figure 16. LEIS mappings of (a) pure MAO/EP, (b) EPM2 (MSN doped in epoxy layer), and (c) EPM1 (MSN filled in MAO layer) coatings in 3.5 wt.% NaCl solution and the impedance values at $x = 1.4$ mm. (With permission from Ref. [140] under a Creative Commons license, Elsevier, open access).

The loading efficiency of corrosion inhibitors in nanocontainers and the maximum doping amount of nanocontainers in polymer resins limit the long-term behavior of those active anti-corrosion composite coatings. Therefore, using the pores and structural defects of PEO coatings as containers for corrosion inhibitor has been proposed [136–139]. Two different ionic liquid corrosion inhibitors, N-(5-hydroxypent-3-yl)-N,N-dimethylhexadecan-1-aminium bromide (N-16) [138] and 1-(3-((N-n-butyl)aminocarboxamido)propyl)-3-hexadecyl imidazolidine bromide (M-16) [136,137,139], are filtrated into the pores of MAO coatings on AZ31 magnesium alloys. Then sealing layers, including hydrophobic wax [138], commercial epoxy [136], and self-healing polyurethanes modified by disulfide bonds [139], are sprayed on the top of corrosion inhibitor loaded MAO coatings. Localized corrosion behaviors in the scratched regions on the damaged and healed coatings were studied by scanning electrochemical microscopy (SECM) measurements, as shown in Figure 17. After heating healing, both the MP-i (MAO/corrosion inhibitor/polyurethane) and MP-0 (MAO/polyurethane) samples exhibit very low tip currents, indicating there is no obvious corrosion activity, while the MP-i sample demonstrates a better self-healing behavior. On the other hand, the corrosion activity

is evident along the scratched area on the surface of the P-i (corrosion inhibitor is loaded in polyurethane without MAO layer) sample, as indicated by the higher tip current and larger corroded area. Table 4 highlights several composite coatings prepared with PEO and organic paint which achieved excellent wear/corrosion protection.

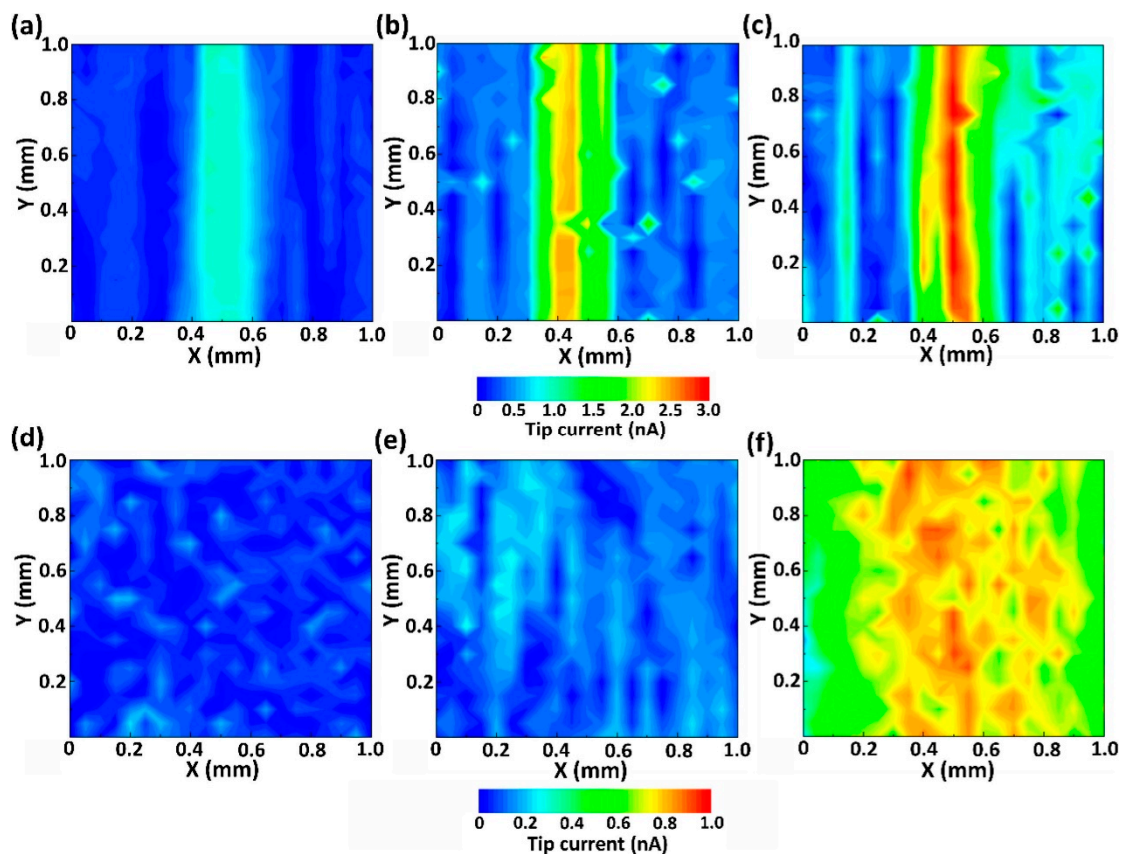


Figure 17. SECM maps of the scratched surfaces for (a) MP-i, (b) MP-0, and (c) P-i samples immersed in 3.5 wt% NaCl solution for 3 days and the healed surfaces for (d) MP-i, (e) MP-0, and (f) P-i samples immersed in 3.5 wt% NaCl solution for 12 days. (With permission from Ref. [139]; License number: 5547411138817, 2023, Elsevier).

Table 4. Several key works with PEO combined with organic paint.

Top Coat	Substrate	Method	Achieved Functions	Ref
Epoxy-silane	ZE41	PEO + Dipping	Excellent corrosion resistance ($10^9 \Omega$) after immersed in NaCl for 31 days	[34]
Mg-rich epoxy primer	Pure Mg	PEO + spray	Excellent corrosion resistance ($10^{10} \Omega$) after 2400 h salt spray test	[141]
PAI + PTFE	AZ31	PEO + spray	Excellent self-lubricating (COF < 0.1) and corrosion resistance	[132]
M16 + polyurethane	AZ31	PEO + dipping + spray	Self-healing and excellent anti-corrosion behavior	[139]
Corrosion inhibitor loaded MSNs + epoxy	AZ31	PEO + dipping + spray	Excellent active protection when MSNs filled in pores of MAO layer, excellent anti-corrosion behavior when MSNs dispersed in epoxy layer	[140]

3. Outlooks for Future Studies

With the understandings provided in the present review, one may suggest some outlooks for future studies. Despite the substantial amount of published research, none of the coatings developed using particle-addition in electrolyte have reached commercial utilization yet, which could be related to the challenge of achieving stable and uniform dispersion, particularly in large industrial treatment baths. Moreover, repeated use of the electrolyte could deteriorate the coating quality due to the depletion of the particles. However, no quantitative information concerning this issue is available yet and more research efforts are needed. Therefore, research on achieving long-term stable and uniform dispersion of adding particles in the electrolyte is urgently needed to put forward the industrial application of MAO coatings on magnesium alloys. A further outlook is related to the repeated usage of electrolyte with particles addition. Moreover, incorporation of more additives and nanoparticles, forming a combined texture of soft and hard particles, in order to improve tribological properties is suggested for future investigations.

Although the corrosion resistance of magnesium alloys is enhanced by PEO coatings, the improvement is still not enough for usage under harsh environments. The authors believe that duplex PEO/post-treatment might provide sufficient corrosion protection. Yet, the impacts of duplex processes on the environment need to be studied. Developing green corrosion inhibitors with excellent corrosion inhibition efficiency might be helpful. Most of the researchers study the tribological and/or corrosion behaviors of duplex PEO-based composite coatings separately. In contrast, there is clear a synergetic effect between wear and corrosion. Additionally, engineering components may work under harsh environments where wear and corrosion exist simultaneously. Therefore, evaluation of the tribocorrosion behavior and/or wear behavior under corrosive circumstances is inevitably required.

Author Contributions: Writing—original draft preparation, C.Z. and X.W.; Writing—review and editing, Supervision, Q.Y., B.Y.; Funding Acquisition, Q.Y., B.Y., M.C. and F.Z.; Project Administration, M.C. and F.Z. All authors have read and agreed to the published version of the manuscript.

Funding: This work is financially supported by National Science Foundation of China (52075524 and 21972153), Youth Innovation Promotion Association CAS (2022429 and 2018454), Gansu Province Science and Technology Plan (22JR5RA094), and Project ZR2022ZD09 supported by Shandong Provincial Natural Science Foundation.

Data Availability Statement: The data used to support the study can be available upon request to the corresponding author.

Conflicts of Interest: The authors declare no conflict of interest.

References

1. Sillekens, W.H.; Hort, N. Magnesium and Magnesium Alloys. In *Structural Materials and Processes in Transportation*; Lehmuhs, D., Busse, M., Herrmann, A.S., Kayvantash, K., Eds.; Wiley-VCH: Weinheim, Germany, 2013; pp. 113–150. [\[CrossRef\]](#)
2. Song, J.; She, J.; Chen, D.; Pan, F. Latest Research Advances on Magnesium and Magnesium Alloys Worldwide. *J. Magnes. Alloy.* **2020**, *8*, 1–41. [\[CrossRef\]](#)
3. Mordike, B.L.; Ebert, T. Magnesium: Properties—Applications—Potential. *Mater. Sci. Eng. A* **2001**, *302*, 37–45. [\[CrossRef\]](#)
4. Song, G.; Atrens, A. Understanding Magnesium Corrosion—A Framework for Improved Alloy Performance. *Adv. Eng. Mater.* **2003**, *5*, 837–858. [\[CrossRef\]](#)
5. Atrens, A.; Song, G.L.; Liu, M.; Shi, Z.; Cao, F.; Dargusch, M.S. Review of Recent Developments in the Field of Magnesium Corrosion. *Adv. Eng. Mater.* **2015**, *17*, 400–453. [\[CrossRef\]](#)
6. Altun, H.; Sen, S. The Effect of DC Magnetron Sputtering AlN Coatings on the Corrosion Behaviour of Magnesium Alloys. *Surf. Coat. Technol.* **2005**, *197*, 193–200. [\[CrossRef\]](#)
7. Zaharescu, M.; Predoana, L.; Barau, A.; Raps, D.; Gammel, F.; Rosero-Navarro, N.C.; Castro, Y.; Durán, A.; Aparicio, M. SiO₂ Based Hybrid Inorganic–Organic Films Doped with TiO₂–CeO₂ Nanoparticles for Corrosion Protection of AA2024 and Mg–AZ31B Alloys. *Corros. Sci.* **2009**, *51*, 1998–2005. [\[CrossRef\]](#)
8. Hoche, H.; Groß, S.; Oechsner, M. Development of New PVD Coatings for Magnesium Alloys with Improved Corrosion Properties. *Surf. Coat. Technol.* **2014**, *259*, 102–108. [\[CrossRef\]](#)
9. Wang, H.; Akid, R.; Gobara, M. Scratch-Resistant Anticorrosion Sol–Gel Coating for the Protection of AZ31 Magnesium Alloy via a Low Temperature Sol–Gel Route. *Corros. Sci.* **2010**, *52*, 2565–2570. [\[CrossRef\]](#)

10. Galio, A.F.; Lamaka, S.V.; Zheludkevich, M.L.; Dick, L.F.P.; Müller, I.L.; Ferreira, M.G.S. Inhibitor-Doped Sol–Gel Coatings for Corrosion Protection of Magnesium Alloy AZ31. *Surf. Coat. Technol.* **2010**, *204*, 1479–1486. [[CrossRef](#)]
11. Bakkar, A.; Neubert, V. Electrodeposition onto Magnesium in Air and Water Stable Ionic Liquids: From Corrosion to Successful Plating. *Electrochem. Commun.* **2007**, *9*, 2428–2435. [[CrossRef](#)]
12. Wu, L.; Zhao, J.; Xie, Y.; Yang, Z. Progress of Electroplating and Electroless Plating on Magnesium Alloy. *Trans. Nonferrous Met. Soc. China* **2010**, *20*, s630–s637. [[CrossRef](#)]
13. El Mahallawy, N.; Bakkar, A.; Shoeib, M.; Palkowski, H.; Neubert, V. Electroless Ni–P Coating of Different Magnesium Alloys. *Surf. Coat. Technol.* **2008**, *202*, 5151–5157. [[CrossRef](#)]
14. Ishihara, S.; Notoya, H.; Okada, A.; Nan, Z.Y.; Goshima, T. Effect of Electroless-Ni-Plating on Corrosion Fatigue Behavior of Magnesium Alloy. *Surf. Coat. Technol.* **2008**, *202*, 2085–2092. [[CrossRef](#)]
15. Tabish, M.; Zhao, J.; Anjum, M.J.; Jingbao, W.; Yasin, G. Self-Healing Self-Healing Chromate-Free Conversion Coatings. In *Conversion Coatings for Magnesium and Its Alloys*; Saji, V.S., Sankara Narayanan, T.S.N., Chen, X., Eds.; Springer International Publishing: Cham, Switzerland, 2022; pp. 299–314; ISBN 978-3-030-89976-9.
16. Wang, X.-M.; Zhang, Z.-Q.; Li, S.-Q.; Kannan, M.B.; Zeng, R.-C. Chemical Conversion Coatings Chemical Conversion Coatings: Fundamentals and Recent Advances. In *Conversion Coatings for Magnesium and Its Alloys*; Saji, V.S., Sankara Narayanan, T.S.N., Chen, X., Eds.; Springer International Publishing: Cham, Switzerland, 2022; pp. 3–28; ISBN 978-3-030-89976-9.
17. Saji, V.S. Organic Conversion Coatings for Magnesium and Its Alloys. *J. Ind. Eng. Chem.* **2019**, *75*, 20–37. [[CrossRef](#)]
18. Wang, G.; Song, D.; Qiao, Y.; Cheng, J.; Liu, H.; Jiang, J.; Ma, A.; Ma, X. Developing Super-Hydrophobic and Corrosion-Resistant Coating on Magnesium-Lithium Alloy via One-Step Hydrothermal Processing. *J. Magnes. Alloy.* **2021**, *11*, 1422–1439. [[CrossRef](#)]
19. Liu, X.; Zhang, T.C.; He, H.; Ouyang, L.; Yuan, S. A Stearic Acid/CeO₂ Bilayer Coating on AZ31B Magnesium Alloy with Superhydrophobic and Self-Cleaning Properties for Corrosion Inhibition. *J. Alloys Compd.* **2020**, *834*, 155210. [[CrossRef](#)]
20. Liu, Y.; Yin, X.; Zhang, J.; Yu, S.; Han, Z.; Ren, L. A Electro-Deposition Process for Fabrication of Biomimetic Super-Hydrophobic Surface and Its Corrosion Resistance on Magnesium Alloy. *Electrochim. Acta* **2014**, *125*, 395–403. [[CrossRef](#)]
21. Chakradhar, R.P.S.; Chandra Mouli, G.; Barshilia, H.; Srivastava, M. Improved Corrosion Protection of Magnesium Alloys AZ31B and AZ91 by Cold-Sprayed Aluminum Coatings. *J. Therm. Spray. Technol.* **2021**, *30*, 371–384. [[CrossRef](#)]
22. Saji, V.S. Review of Rare-Earth-Based Conversion Coatings for Magnesium and Its Alloys. *J. Mater. Res. Technol.* **2019**, *8*, 5012–5035. [[CrossRef](#)]
23. Hu, H.; Nie, X.; Ma, Y. Corrosion and Surface Treatment of Magnesium Alloys. In *Magnesium Alloys-Properties in Solid and Liquid States*; IntechOpen: London, UK, 2014. [[CrossRef](#)]
24. Vijh, A.K. Sparking Voltages and Side Reactions during Anodization of Valve Metals in Terms of Electron Tunnelling. *Corros. Sci.* **1971**, *11*, 411–417. [[CrossRef](#)]
25. Wang, L.; Chen, L.; Yan, Z.; Fu, W. Optical Emission Spectroscopy Studies of Discharge Mechanism and Plasma Characteristics during Plasma Electrolytic Oxidation of Magnesium in Different Electrolytes. *Surf. Coat. Technol.* **2010**, *205*, 1651–1658. [[CrossRef](#)]
26. Yerokhin, A.L.; Snizhko, L.O.; Gurevina, N.L.; Leyland, A.; Pilkington, A.; Matthews, A. Discharge Characterization in Plasma Electrolytic Oxidation of Aluminium. *J. Phys. D Appl. Phys.* **2003**, *36*, 2110. [[CrossRef](#)]
27. Curran, J.A.; Clyne, T.W. Porosity in Plasma Electrolytic Oxide Coatings. *Acta Mater.* **2006**, *54*, 1985–1993. [[CrossRef](#)]
28. Hussein, R.O.; Nie, X.; Northwood, D.O.; Yerokhin, A.; Matthews, A. Spectroscopic Study of Electrolytic Plasma and Discharging Behaviour during the Plasma Electrolytic Oxidation (PEO) Process. *J. Phys. D Appl. Phys.* **2010**, *43*, 105203. [[CrossRef](#)]
29. Krysmann, W.; Kurze, P.; Dittrich, K.-H.; Schneider, H.G. Process Characteristics and Parameters of Anodic Oxidation by Spark Discharge (ANOF). *Crysl. Res. Technol.* **1984**, *19*, 973–979. [[CrossRef](#)]
30. Ikonopisov, S. Theory of Electrical Breakdown during Formation of Barrier Anodic Films. *Electrochim. Acta* **1977**, *22*, 1077–1082. [[CrossRef](#)]
31. Mécuson, F.; Czerwiec, T.; Belmonte, T.; Dujardin, L.; Viola, A.; Henrion, G. Diagnostics of an Electrolytic Microarc Process for Aluminium Alloy Oxidation. *Surf. Coat. Technol.* **2005**, *200*, 804–808. [[CrossRef](#)]
32. Hussein, R.O.; Nie, X.; Northwood, D.O. An Investigation of Ceramic Coating Growth Mechanisms in Plasma Electrolytic Oxidation (PEO) Processing. *Electrochim. Acta* **2013**, *112*, 111–119. [[CrossRef](#)]
33. Barati Darband, G.; Aliofkhaezrai, M.; Hamghalam, P.; Valizade, N. Plasma Electrolytic Oxidation of Magnesium and Its Alloys: Mechanism, Properties and Applications. *J. Magnes. Alloy.* **2017**, *5*, 74–132. [[CrossRef](#)]
34. Ivanou, D.K.; Sarykevich, M.; Lisenkov, A.D.; Zheludkevich, M.L.; Xue, H.B.; Lamaka, S.V.; Ferreira, M.G.S. Plasma Anodized ZE41 Magnesium Alloy Sealed with Hybrid Epoxy-Silane Coating. *Corros. Sci.* **2013**, *73*, 300–308. [[CrossRef](#)]
35. Hussein, R.; Xueyuan, N.; Derek, N. The Application of Plasma Electrolytic Oxidation (PEO) to the Production of Corrosion Resistant Coatings on Magnesium Alloys: A Review. *Corros. Mater.* **2013**, *38*, 54–65.
36. Kaseem, M.; Dikici, B. Optimization of Surface Properties of Plasma Electrolytic Oxidation Coating by Organic Additives: A Review. *Coatings* **2021**, *11*, 374. [[CrossRef](#)]
37. Shahri, Z.; Allahkaram, S.R.; Soltani, R.; Jafari, H. Optimization of Plasma Electrolyte Oxidation Process Parameters for Corrosion Resistance of Mg Alloy. *J. Magnes. Alloy.* **2020**, *8*, 431–440. [[CrossRef](#)]
38. Hussein, R.O.; Northwood, D.O.; Nie, X. The Effect of Processing Parameters and Substrate Composition on the Corrosion Resistance of Plasma Electrolytic Oxidation (PEO) Coated Magnesium Alloys. *Surf. Coat. Technol.* **2013**, *237*, 357–368. [[CrossRef](#)]

39. Fattah-alhosseini, A.; Chaharmahali, R.; Babaei, K. Effect of Particles Addition to Solution of Plasma Electrolytic Oxidation (PEO) on the Properties of PEO Coatings Formed on Magnesium and Its Alloys: A Review. *J. Magnes. Alloy.* **2020**, *8*, 799–818. [[CrossRef](#)]
40. Lu, X.; Mohedano, M.; Blawert, C.; Matykina, E.; Arrabal, R.; Kainer, K.U.; Zheludkevich, M.L. Plasma Electrolytic Oxidation Coatings with Particle Additions—A Review. *Surf. Coat. Technol.* **2016**, *307*, 1165–1182. [[CrossRef](#)]
41. Rapheal, G.; Kumar, S.; Scharnagl, N.; Blawert, C. Effect of Current Density on the Microstructure and Corrosion Properties of Plasma Electrolytic Oxidation (PEO) Coatings on AM50 Mg Alloy Produced in an Electrolyte Containing Clay Additives. *Surf. Coat. Technol.* **2016**, *289*, 150–164. [[CrossRef](#)]
42. Lu, X.; Blawert, C.; Mohedano, M.; Scharnagl, N.; Zheludkevich, M.L.; Kainer, K.U. Influence of Electrical Parameters on Particle Uptake during Plasma Electrolytic Oxidation Processing of AM50 Mg Alloy. *Surf. Coat. Technol.* **2016**, *289*, 179–185. [[CrossRef](#)]
43. Lu, X.; Sah, S.P.; Scharnagl, N.; Störmer, M.; Starykevich, M.; Mohedano, M.; Blawert, C.; Zheludkevich, M.L.; Kainer, K.U. Degradation Behavior of PEO Coating on AM50 Magnesium Alloy Produced from Electrolytes with Clay Particle Addition. *Surf. Coat. Technol.* **2015**, *269*, 155–169. [[CrossRef](#)]
44. Blawert, C.; Sah, S.P.; Liang, J.; Huang, Y.; Höche, D. Role of Sintering and Clay Particle Additions on Coating Formation during PEO Processing of AM50 Magnesium Alloy. *Surf. Coat. Technol.* **2012**, *213*, 48–58. [[CrossRef](#)]
45. Lu, X.; Blawert, C.; Huang, Y.; Ovri, H.; Zheludkevich, M.L.; Kainer, K.U. Plasma Electrolytic Oxidation Coatings on Mg Alloy with Addition of SiO₂ Particles. *Electrochim. Acta* **2016**, *187*, 20–33. [[CrossRef](#)]
46. Liang, J.; Hu, L.; Hao, J. Preparation and Characterization of Oxide Films Containing Crystalline TiO₂ on Magnesium Alloy by Plasma Electrolytic Oxidation. *Electrochim. Acta* **2007**, *52*, 4836–4840. [[CrossRef](#)]
47. Zhang, D.; Gou, Y.; Liu, Y.; Guo, X. A Composite Anodizing Coating Containing Superfine Al₂O₃ Particles on AZ31 Magnesium Alloy. *Surf. Coat. Technol.* **2013**, *236*, 52–57. [[CrossRef](#)]
48. Laleh, M.; Rouhaghdam, A.S.; Shahrabi, T.; Shanghi, A. Effect of Alumina Sol Addition to Micro-Arc Oxidation Electrolyte on the Properties of MAO Coatings Formed on Magnesium Alloy AZ91D. *J. Alloys Compd.* **2010**, *496*, 548–552. [[CrossRef](#)]
49. Asgari, M.; Aliofkhazraei, M.; Darband, G.H.B.; Rouhaghdam, A.S. Evaluation of Alumina Nanoparticles Concentration and Stirring Rate on Wear and Corrosion Behavior of Nanocomposite PEO Coating on AZ31 Magnesium Alloy. *Surf. Coat. Technol.* **2017**, *309*, 124–135. [[CrossRef](#)]
50. Daroonparvar, M.; Yajid, M.A.M.; Yusof, N.M.; Bakhsheshi-Rad, H.R. Preparation and Corrosion Resistance of a Nanocomposite Plasma Electrolytic Oxidation Coating on Mg-1%Ca Alloy Formed in Aluminate Electrolyte Containing Titania Nano-Additives. *J. Alloys Compd.* **2016**, *688*, 841–857. [[CrossRef](#)]
51. Liu, J.; Lu, Y.; Jing, X.; Yuan, Y.; Zhang, M. Characterization of Plasma Electrolytic Oxidation Coatings Formed on Mg–Li Alloy in an Alkaline Silicate Electrolyte Containing Silica Sol. *Mater. Corros.* **2009**, *60*, 865–870. [[CrossRef](#)]
52. Lee, K.M.; Shin, K.R.; Namgung, S.; Yoo, B.; Shin, D.H. Electrochemical Response of ZrO₂-Incorporated Oxide Layer on AZ91 Mg Alloy Processed by Plasma Electrolytic Oxidation. *Surf. Coat. Technol.* **2011**, *205*, 3779–3784. [[CrossRef](#)]
53. Lim, T.S.; Ryu, H.S.; Hong, S.-H. Electrochemical Corrosion Properties of CeO₂-Containing Coatings on AZ31 Magnesium Alloys Prepared by Plasma Electrolytic Oxidation. *Corros. Sci.* **2012**, *62*, 104–111. [[CrossRef](#)]
54. Mohedano, M.; Blawert, C.; Zheludkevich, M.L. Silicate-Based Plasma Electrolytic Oxidation (PEO) Coatings with Incorporated CeO₂ Particles on AM50 Magnesium Alloy. *Mater. Des.* **2015**, *86*, 735–744. [[CrossRef](#)]
55. Zheng, Z.; Zhao, M.-C.; Tan, L.; Zhao, Y.-C.; Xie, B.; Yin, D.; Yang, K.; Atrens, A. Corrosion Behavior of a Self-Sealing Coating Containing CeO₂ Particles on Pure Mg Produced by Micro-Arc Oxidation. *Surf. Coat. Technol.* **2020**, *386*, 125456. [[CrossRef](#)]
56. Guo, J.; Wang, L.; Wang, S.C.; Liang, J.; Xue, Q.; Yan, F. Preparation and Performance of a Novel Multifunctional Plasma Electrolytic Oxidation Composite Coating Formed on Magnesium Alloy. *J. Mater. Sci.* **2009**, *44*, 1998–2006. [[CrossRef](#)]
57. Zhao, J.; Xie, X.; Zhang, C. Effect of the Graphene Oxide Additive on the Corrosion Resistance of the Plasma Electrolytic Oxidation Coating of the AZ31 Magnesium Alloy. *Corros. Sci.* **2017**, *114*, 146–155. [[CrossRef](#)]
58. Wang, Y.; Wei, D.; Yu, J.; Di, S. Effects of Al₂O₃ Nano-Additive on Performance of Micro-Arc Oxidation Coatings Formed on AZ91D Mg Alloy. *J. Mater. Sci. Technol.* **2014**, *30*, 984–990. [[CrossRef](#)]
59. Tang, M.; Liu, H.; Li, W.; Zhu, L. Effect of Zirconia Sol in Electrolyte on the Characteristics of Microarc Oxidation Coating on AZ91D Magnesium. *Mater. Lett.* **2011**, *65*, 413–415. [[CrossRef](#)]
60. Yu, L.; Cao, J.; Cheng, Y. An Improvement of the Wear and Corrosion Resistances of AZ31 Magnesium Alloy by Plasma Electrolytic Oxidation in a Silicate–Hexametaphosphate Electrolyte with the Suspension of SiC Nanoparticles. *Surf. Coat. Technol.* **2015**, *276*, 266–278. [[CrossRef](#)]
61. Zhang, R.F.; Zhang, S.F.; Yang, N.; Yao, L.J.; He, F.X.; Zhou, Y.P.; Xu, X.; Chang, L.; Bai, S.J. Influence of 8-Hydroxyquinoline on Properties of Anodic Coatings Obtained by Micro Arc Oxidation on AZ91 Magnesium Alloys. *J. Alloys Compd.* **2012**, *539*, 249–255. [[CrossRef](#)]
62. Küçükosman, R.; Emine Şüküroğlu, E.; Totik, Y.; Şüküroğlu, S. Investigation of Wear Behavior of Graphite Additive Composite Coatings Deposited by Micro Arc Oxidation-Hydrothermal Treatment on AZ91 Mg Alloy. *Surf. Interfaces* **2021**, *22*, 100894. [[CrossRef](#)]
63. Erdil, M.; Aydın, F. Influence of Graphene Particles on the Wear and Corrosion Performance of MAO Produced AZ31 Alloy. *Fuller. Nanotub. Carbon Nanostruct.* **2021**, *29*, 998–1008. [[CrossRef](#)]

64. Lou, B.-S.; Lee, J.-W.; Tseng, C.-M.; Lin, Y.-Y.; Yen, C.-A. Mechanical Property and Corrosion Resistance Evaluation of AZ31 Magnesium Alloys by Plasma Electrolytic Oxidation Treatment: Effect of MoS₂ Particle Addition. *Surf. Coat. Technol.* **2018**, *350*, 813–822. [[CrossRef](#)]
65. NasiriVatan, H.; Ebrahimi-Kahrizsangi, R.; Asgarani, M.K. Tribological Performance of PEO-WC Nanocomposite Coating on Mg Alloys Deposited by Plasma Electrolytic Oxidation. *Tribol. Int.* **2016**, *98*, 253–260. [[CrossRef](#)]
66. Lou, B.-S.; Lin, Y.-Y.; Tseng, C.-M.; Lu, Y.-C.; Duh, J.-G.; Lee, J.-W. Plasma Electrolytic Oxidation Coatings on AZ31 Magnesium Alloys with Si₃N₄ Nanoparticle Additives. *Surf. Coat. Technol.* **2017**, *332*, 358–367. [[CrossRef](#)]
67. Mashtalyar, D.V.; Sinebryukhov, S.L.; Imshinetskiy, I.M.; Gnedenkov, A.S.; Nadaraia, K.V.; Ustinov, A.Y.; Gnedenkov, S.V. Hard Wearproof PEO-Coatings Formed on Mg Alloy Using TiN Nanoparticles. *Appl. Surf. Sci.* **2020**, *503*, 144062. [[CrossRef](#)]
68. Li, Y.; Lu, X.; Serdechnova, M.; Blawert, C.; Zheludkevich, M.L.; Qian, K.; Zhang, T.; Wang, F. Incorporation of LDH Nanocontainers into Plasma Electrolytic Oxidation Coatings on Mg Alloy. *J. Magnes. Alloy.* **2021**, *11*, 1236–1246. [[CrossRef](#)]
69. Sun, M.; Yerokhin, A.; Bychkova, M.Y.; Shtansky, D.V.; Levashov, E.A.; Matthews, A. Self-Healing Plasma Electrolytic Oxidation Coatings Doped with Benzotriazole Loaded Halloysite Nanotubes on AM50 Magnesium Alloy. *Corros. Sci.* **2016**, *111*, 753–769. [[CrossRef](#)]
70. Wu, W.X.; Wang, W.P.; Lin, H.C. A Study on Corrosion Behavior of Micro-Arc Oxidation Coatings Doped with 2-Aminobenzimidazole Loaded Halloysite Nanotubes on AZ31 Magnesium Alloys. *Surf. Coat. Technol.* **2021**, *416*, 127116. [[CrossRef](#)]
71. Udoh, I.I.; Shi, H.; Daniel, E.F.; Li, J.; Gu, S.; Liu, F.; Han, E.-H. Active Anticorrosion and Self-Healing Coatings: A Review with Focus on Multi-Action Smart Coating Strategies. *J. Mater. Sci. Technol.* **2022**, *116*, 224–237. [[CrossRef](#)]
72. Rapheal, G.; Kumar, S.; Blawert, C.; Dahotre, N.B. Wear Behavior of Plasma Electrolytic Oxidation (PEO) and Hybrid Coatings of PEO and Laser on MRI 230D Magnesium Alloy. *Wear* **2011**, *271*, 1987–1997. [[CrossRef](#)]
73. Habibi, M.; Miresmaeili, R.; Aliofkhaezrai, M.; Chamgordani, S.A. Laser Melting Effects on Microstructure and Corrosion Behavior of Plasma Electrolytic Oxidation Nanocomposite Coatings on Pure Titanium. *Procedia Mater. Sci.* **2015**, *11*, 491–497. [[CrossRef](#)]
74. Liang, J.; Wang, P.; Hu, L.; Hao, J. Tribological Properties of Duplex MAO/DLC Coatings on Magnesium Alloy Using Combined Microarc Oxidation and Filtered Cathodic Arc Deposition. *Mater. Sci. Eng. A* **2007**, *454–455*, 164–169. [[CrossRef](#)]
75. Yang, W.; Ke, P.; Fang, Y.; Zheng, H.; Wang, A. Microstructure and Properties of Duplex (Ti:N)-DLC/MAO Coating on Magnesium Alloy. *Appl. Surf. Sci.* **2013**, *270*, 519–525. [[CrossRef](#)]
76. Ning, C.-M.; Cui, X.-J.; Shang, L.-L.; Zhang, Y.-J.; Zhang, G.-A. Structure and Properties of Different Elements Doped Diamond-like Carbon on Micro-Arc Oxidation Coated AZ31B Mg Alloy. *Diam. Relat. Mater.* **2020**, *106*, 107832. [[CrossRef](#)]
77. Sun, M.; Yerokhin, A.; Matthews, A.; Thomas, M.; Laukart, A.; von Hausen, M.; Klages, C.-P. Characterisation and Electrochemical Evaluation of Plasma Electrolytic Oxidation Coatings on Magnesium with Plasma Enhanced Chemical Vapour Deposition Post-Treatments. *Plasma Process. Polym.* **2016**, *13*, 266–278. [[CrossRef](#)]
78. Gu, C.; Lian, J.; Li, G.; Niu, L.; Jiang, Z. Electroless Ni-P Plating on AZ91D Magnesium Alloy from a Sulfate Solution. *J. Alloys Compd.* **2005**, *391*, 104–109. [[CrossRef](#)]
79. Ambat, R.; Zhou, W. Electroless Nickel-Plating on AZ91D Magnesium Alloy: Effect of Substrate Microstructure and Plating Parameters. *Surf. Coat. Technol.* **2004**, *179*, 124–134. [[CrossRef](#)]
80. Liu, Z.; Gao, W. A Novel Process of Electroless Ni-P Plating with Plasma Electrolytic Oxidation Pretreatment. *Appl. Surf. Sci.* **2006**, *253*, 2988–2991. [[CrossRef](#)]
81. Zeng, L.; Yang, S.; Zhang, W.; Guo, Y.; Yan, C. Preparation and Characterization of a Double-Layer Coating on Magnesium Alloy AZ91D. *Electrochim. Acta* **2010**, *55*, 3376–3383. [[CrossRef](#)]
82. Sun, S.; Liu, J.; Yan, C.; Wang, F. A Novel Process for Electroless Nickel Plating on Anodized Magnesium Alloy. *Appl. Surf. Sci.* **2008**, *254*, 5016–5022. [[CrossRef](#)]
83. Guo, X.; Du, K.; Guo, Q.; Wang, Y.; Wang, F. Experimental Study of Corrosion Protection of a Three-Layer Film on AZ31B Mg Alloy. *Corros. Sci.* **2012**, *65*, 367–375. [[CrossRef](#)]
84. Kannan, M.B.; Walter, R.; Yamamoto, A.; Khakbaz, H.; Blawert, C. Electrochemical Surface Engineering of Magnesium Metal by Plasma Electrolytic Oxidation and Calcium Phosphate Deposition: Biocompatibility and in Vitro Degradation Studies. *RSC Adv.* **2018**, *8*, 29189–29200. [[CrossRef](#)]
85. Han, J.; Tang, S.; San, H.; Sun, X.; Hu, J.; Yu, Y. Formation Mechanism of Calcium Phosphate Coating on a Plasma Electrolytic Oxidized Magnesium and Its Corrosion Behavior in Simulated Body Fluids. *J. Alloys Compd.* **2020**, *818*, 152834. [[CrossRef](#)]
86. Wang, D.; Ma, C.; Liu, J.; Li, W.; Shang, W.; Peng, N.; Wen, Y. Corrosion Resistance and Anti-Soiling Performance of Micro-Arc Oxidation/Graphene Oxide/Stearic Acid Superhydrophobic Composite Coating on Magnesium Alloys. *Int. J. Miner. Metall. Mater.* **2023**, *30*, 1128–1139. [[CrossRef](#)]
87. Sreekanth, D.; Rameshbabu, N. Development and Characterization of MgO/Hydroxyapatite Composite Coating on AZ31 Magnesium Alloy by Plasma Electrolytic Oxidation Coupled with Electrophoretic Deposition. *Mater. Lett.* **2012**, *68*, 439–442. [[CrossRef](#)]
88. Bordbar Khiabani, A.; Rahimi, S.; Yarmand, B.; Mozafari, M. Electrophoretic Deposition of Graphene Oxide on Plasma Electrolytic Oxidized-Magnesium Implants for Bone Tissue Engineering Applications. *Mater. Today Proc.* **2018**, *5*, 15603–15612. [[CrossRef](#)]

89. Gnedenkov, S.V.; Sinebryukhov, S.L.; Mashtalyar, D.V.; Imshinetskiy, I.M. Composite Fluoropolymer Coatings on Mg Alloys Formed by Plasma Electrolytic Oxidation in Combination with Electrophoretic Deposition. *Surf. Coat. Technol.* **2015**, *283*, 347–352. [[CrossRef](#)]
90. Jiang, Y.; Bao, Y.; Yang, K. Composite Coatings Combining PEO Layer and EPD Layer on Magnesium Alloy. In *Magnesium Technology 2011*; Sillekens, W.H., Agnew, S.R., Neelameggham, N.R., Mathaudhu, S.N., Eds.; Springer International Publishing: Cham, Switzerland, 2016; pp. 543–546; ISBN 978-3-319-48223-1.
91. Wang, C.; Jiang, B.; Liu, M.; Ge, Y. Corrosion Characterization of Micro-Arc Oxidation Composite Electrophoretic Coating on AZ31B Magnesium Alloy. *J. Alloys Compd.* **2015**, *621*, 53–61. [[CrossRef](#)]
92. Gao, J.H.; Guan, S.K.; Chen, J.; Wang, L.G.; Zhu, S.J.; Hu, J.H.; Ren, Z.W. Fabrication and Characterization of Rod-like Nano-Hydroxyapatite on MAO Coating Supported on Mg–Zn–Ca Alloy. *Appl. Surf. Sci.* **2011**, *257*, 2231–2237. [[CrossRef](#)]
93. Wu, C.; Wen, Z.; Dai, C.; Lu, Y.; Yang, F. Fabrication of Calcium Phosphate/Chitosan Coatings on AZ91D Magnesium Alloy with a Novel Method. *Surf. Coat. Technol.* **2010**, *204*, 3336–3347. [[CrossRef](#)]
94. Shi, Y.; Qi, M.; Chen, Y.; Shi, P. MAO-DCPD Composite Coating on Mg Alloy for Degradable Implant Applications. *Mater. Lett.* **2011**, *65*, 2201–2204. [[CrossRef](#)]
95. Shang, W.; Chen, B.; Shi, X.; Chen, Y.; Xiao, X. Electrochemical Corrosion Behavior of Composite MAO/Sol–Gel Coatings on Magnesium Alloy AZ91D Using Combined Micro-Arc Oxidation and Sol–Gel Technique. *J. Alloys Compd.* **2009**, *474*, 541–545. [[CrossRef](#)]
96. Li, Z.; Jing, X.; Yuan, Y.; Zhang, M. Composite Coatings on a Mg–Li Alloy Prepared by Combined Plasma Electrolytic Oxidation and Sol–Gel Techniques. *Corros. Sci.* **2012**, *63*, 358–366. [[CrossRef](#)]
97. Guo, X.; An, M. Experimental Study of Electrochemical Corrosion Behaviour of Bilayer on AZ31B Mg Alloy. *Corros. Sci.* **2010**, *52*, 4017–4027. [[CrossRef](#)]
98. Guo, X.; Du, K.; Wang, Y.; Shao, Y.; Wang, F. A New Nanoparticle Penetrant Used for Plasma Electrolytic Oxidation Film Coated on AZ31 Mg Alloy in Service Environment. *Surf. Coat. Technol.* **2012**, *206*, 4833–4839. [[CrossRef](#)]
99. Li, N.; Chen, Y.; Deng, B.; Yue, J.; Qu, W.; Yang, H.; He, Y.; Xia, W.; Li, L. Low Temperature UV Assisted Sol-Gel Preparation of ZrO₂ Pore-Sealing Films on Micro-Arc Oxidized Magnesium Alloy AZ91D and Their Electrochemical Corrosion Behaviors. *J. Alloys Compd.* **2019**, *792*, 1036–1044. [[CrossRef](#)]
100. Merino, E.; Durán, A.; Castro, Y. Integrated Corrosion-Resistant System for AZ31B Mg Alloy via Plasma Electrolytic Oxidation (PEO) and Sol-Gel Processes. *Int. J. Appl. Glass Sci.* **2021**, *12*, 519–530. [[CrossRef](#)]
101. Pezzato, L.; Rigon, M.; Martucci, A.; Brunelli, K.; Dabalà, M. Plasma Electrolytic Oxidation (PEO) as Pre-Treatment for Sol-Gel Coating on Aluminum and Magnesium Alloys. *Surf. Coat. Technol.* **2019**, *366*, 114–123. [[CrossRef](#)]
102. Telmenbayar, L.; Ramu, A.G.; Erdenebat, T.-O.; Choi, D. Anticorrosive Lanthanum Embedded PEO/GPTMS Coating on Magnesium Alloy by Plasma Electrolytic Oxidation with Silanization. *Mater. Today Commun.* **2022**, *33*, 104662. [[CrossRef](#)]
103. Li, T.; Sun, F.; Zhao, Y.; Chen, M. The Corrosion Resistance of SiO₂-Hexadecyltrimethoxysilane Hydrophobic Coating on AZ91 Alloy Pretreated by Plasma Electrolytic Oxidation. *Prog. Org. Coat.* **2023**, *174*, 107232. [[CrossRef](#)]
104. Shi, P.; Ng, W.F.; Wong, M.H.; Cheng, F.T. Improvement of Corrosion Resistance of Pure Magnesium in Hanks' Solution by Microarc Oxidation with Sol–Gel TiO₂ Sealing. *J. Alloys Compd.* **2009**, *469*, 286–292. [[CrossRef](#)]
105. Ivanou, D.K.; Yasakau, K.A.; Kallip, S.; Lisenkov, A.D.; Starykevich, M.; Lamaka, S.V.; Ferreira, M.G.S.; Zheludkevich, M.L. Active Corrosion Protection Coating for a ZE41 Magnesium Alloy Created by Combining PEO and Sol–Gel Techniques. *RSC Adv.* **2016**, *6*, 12553–12560. [[CrossRef](#)]
106. Qiu, Z.; Sun, J.; Wang, R.; Zhang, Y.; Wu, X. Magnet-Induced Fabrication of a Superhydrophobic Surface on ZK60 Magnesium Alloy. *Surf. Coat. Technol.* **2016**, *286*, 246–250. [[CrossRef](#)]
107. Chen, Y.; Lu, X.; Lamaka, S.V.; Ju, P.; Blawert, C.; Zhang, T.; Wang, F.; Zheludkevich, M.L. Active Protection of Mg Alloy by Composite PEO Coating Loaded with Corrosion Inhibitors. *Appl. Surf. Sci.* **2020**, *504*, 144462. [[CrossRef](#)]
108. Chang, L.; Tian, L.; Liu, W.; Duan, X. Formation of Dicalcium Phosphate Dihydrate on Magnesium Alloy by Micro-Arc Oxidation Coupled with Hydrothermal Treatment. *Corros. Sci.* **2013**, *72*, 118–124. [[CrossRef](#)]
109. Yao, Z.; Xia, Q.; Chang, L.; Li, C.; Jiang, Z. Structure and Properties of Compound Coatings on Mg Alloys by Micro-Arc Oxidation/Hydrothermal Treatment. *J. Alloys Compd.* **2015**, *633*, 435–442. [[CrossRef](#)]
110. Zhang, G.; Wu, L.; Serdechnova, M.; Tang, A.; Wang, C.; Blawert, C.; Pan, F.; Zheludkevich, M.L. In-Situ LDHs Growth on PEO Coatings on AZ31 Magnesium Alloy for Active Protection: Roles of PEO Composition and Conversion Solution. *J. Magnes. Alloy.* **2021**. [[CrossRef](#)]
111. Chen, Y.; Wu, L.; Yao, W.; Wu, J.; Yuan, Y.; Xie, Z.; Jiang, B.; Pan, F. Synergistic Effect of Graphene Oxide/Ternary Mg–Al–La Layered Double Hydroxide for Dual Self-Healing Corrosion Protection of Micro-Arc Oxide Coating of Magnesium Alloy. *Colloids Surf. A Phys. Eng. Asp.* **2022**, *655*, 130339. [[CrossRef](#)]
112. Chen, Y.; Wu, L.; Yao, W.; Chen, Y.; Zhong, Z.; Ci, W.; Wu, J.; Xie, Z.; Yuan, Y.; Pan, F. A Self-Healing Corrosion Protection Coating with Graphene Oxide Carrying 8-Hydroxyquinoline Doped in Layered Double Hydroxide on a Micro-Arc Oxidation Coating. *Corros. Sci.* **2022**, *194*, 109941. [[CrossRef](#)]
113. Chen, Y.; Wu, L.; Yao, W.; Wu, J.; Yuan, Y.; Jiang, B.; Pan, F. Growth Behavior and Corrosion Resistance of Graphene Oxide/MgAl Layered Double Hydroxide Coating Grown on Micro-Arc Oxidation Film of Magnesium Alloys. *J. Ind. Eng. Chem.* **2023**, *117*, 319–332. [[CrossRef](#)]

114. Zhang, G.; Jiang, E.; Wu, L.; Tang, A.; Atrens, A.; Pan, F. Active Corrosion Protection of Phosphate Loaded PEO/LDHs Composite Coatings: SIET Study. *J. Magnes. Alloy.* **2022**, *10*, 1351–1357. [[CrossRef](#)]
115. Toro, L.; Zuleta, A.A.; Correa, E.; Echeverría, F. Hydrothermal Sealing of Plasma Electrolytic Oxidation Coatings Developed on AZ31 Alloy. *J. Mater. Eng. Perform.* **2022**, *31*, 9768–9776. [[CrossRef](#)]
116. Dou, J.; Wang, J.; Li, H.; Lu, Y.; Yu, H.; Chen, C. Enhanced Corrosion Resistance of Magnesium Alloy by Plasma Electrolytic Oxidation plus Hydrothermal Treatment. *Surf. Coat. Technol.* **2021**, *424*, 127662. [[CrossRef](#)]
117. Chen, Y.; Wu, L.; Yao, W.; Wu, J.; Xiang, J.; Dai, X.; Wu, T.; Yuan, Y.; Wang, J.; Jiang, B.; et al. Development of Metal-Organic Framework (MOF) Decorated Graphene Oxide/MgAl-Layered Double Hydroxide Coating via Microstructural Optimization for Anti-Corrosion Micro-Arc Oxidation Coatings of Magnesium Alloy. *J. Mater. Sci. Technol.* **2022**, *130*, 12–26. [[CrossRef](#)]
118. Chen, Y.; Wu, L.; Yao, W.; Wu, J.; Xie, Z.; Yuan, Y.; Jiang, B.; Pan, F. In Situ Growth of Mg-Zn-Al LDHs by ZIF-8 Carrying Zn Source and Micro-Arc Oxidation Integrated Coating for Corrosion and Protection of Magnesium Alloys. *Surf. Coat. Technol.* **2022**, *451*, 129032. [[CrossRef](#)]
119. Yu, W.; Sun, R.; Guo, Z.; Wang, Z.; He, Y.; Lu, G.; Chen, P.; Chen, K. Novel Fluoridated Hydroxyapatite/MAO Composite Coating on AZ31B Magnesium Alloy for Biomedical Application. *Appl. Surf. Sci.* **2019**, *464*, 708–715. [[CrossRef](#)]
120. Wang, H.; Song, Y.; Chen, X.; Tong, G.; Zhang, L. Microstructure and Corrosion Behavior of PEO-LDHs-SDS Superhydrophobic Composite Film on Magnesium Alloy. *Corros. Sci.* **2022**, *208*, 110699. [[CrossRef](#)]
121. Wu, L.; Wu, J.; Zhang, Z.; Zhang, C.; Zhang, Y.; Tang, A.; Li, L.; Zhang, G.; Zheng, Z.; Atrens, A.; et al. Corrosion Resistance of Fatty Acid and Fluoroalkylsilane-Modified Hydrophobic Mg-Al LDH Films on Anodized Magnesium Alloy. *Appl. Surf. Sci.* **2019**, *487*, 569–580. [[CrossRef](#)]
122. Peng, F.; Wang, D.; Tian, Y.; Cao, H.; Qiao, Y.; Liu, X. Sealing the Pores of PEO Coating with Mg-Al Layered Double Hydroxide: Enhanced Corrosion Resistance, Cytocompatibility and Drug Delivery Ability. *Sci. Rep.* **2017**, *7*, 8167. [[CrossRef](#)]
123. Zhang, G.; Wu, L.; Tang, A.; Chen, X.-B.; Ma, Y.; Long, Y.; Peng, P.; Ding, X.; Pan, H.; Pan, F. Growth Behavior of MgAl-Layered Double Hydroxide Films by Conversion of Anodic Films on Magnesium Alloy AZ31 and Their Corrosion Protection. *Appl. Surf. Sci.* **2018**, *456*, 419–429. [[CrossRef](#)]
124. Zhang, G.; Wu, L.; Tang, A.; Ma, Y.; Song, G.-L.; Zheng, D.; Jiang, B.; Atrens, A.; Pan, F. Active Corrosion Protection by a Smart Coating Based on a MgAl-Layered Double Hydroxide on a Cerium-Modified Plasma Electrolytic Oxidation Coating on Mg Alloy AZ31. *Corros. Sci.* **2018**, *139*, 370–382. [[CrossRef](#)]
125. Anjum, M.J.; Zhao, J.; Zahedi Asl, V.; Yasin, G.; Wang, W.; Wei, S.; Zhao, Z.; Qamar Khan, W. In-Situ Intercalation of 8-Hydroxyquinoline in Mg-Al LDH Coating to Improve the Corrosion Resistance of AZ31. *Corros. Sci.* **2019**, *157*, 1–10. [[CrossRef](#)]
126. Wang, J.; Tang, J.; He, Y. Top Coating of Low-Molecular Weight Polymer MALPB Used for Enhanced Protection on Anodized AZ31B Mg Alloys. *J. Coat. Technol. Res.* **2010**, *7*, 737–746. [[CrossRef](#)]
127. Arrabal, R.; Mota, J.M.; Criado, A.; Pardo, A.; Mohedano, M.; Matykina, E. Assessment of Duplex Coating Combining Plasma Electrolytic Oxidation and Polymer Layer on AZ31 Magnesium Alloy. *Surf. Coat. Technol.* **2012**, *206*, 4692–4703. [[CrossRef](#)]
128. Castellanos, A.; Altube, A.; Vega, J.M.; García-Lecina, E.; Díez, J.A.; Grande, H.J. Effect of Different Post-Treatments on the Corrosion Resistance and Tribological Properties of AZ91D Magnesium Alloy Coated PEO. *Surf. Coat. Technol.* **2015**, *278*, 99–107. [[CrossRef](#)]
129. Cui, X.-J.; Li, M.-T.; Yang, R.-S.; Yu, Z.-X. Structure and Properties of a Duplex Coating Combining Micro-Arc Oxidation and Baking Layer on AZ91D Mg Alloy. *Appl. Surf. Sci.* **2016**, *363*, 91–100. [[CrossRef](#)]
130. Simancas, J.; de la Fuente, D.; Chico, B.; Madueño, L.; Camón, F.; Blanco, M.C.; Morcillo, M. Anticorrosive Behaviour of Cr(VI)-Free Surface Pretreatments Applied on Magnesium Alloys. *Prog. Org. Coat.* **2013**, *76*, 1833–1840. [[CrossRef](#)]
131. Bakhsheshi-Rad, H.R.; Hamzah, E.; Ebrahimi-Kahrizsangi, R.; Daroonparvar, M.; Medraj, M. Fabrication and Characterization of Hydrophobic Microarc Oxidation/Poly-Lactic Acid Duplex Coating on Biodegradable Mg–Ca Alloy for Corrosion Protection. *Vacuum* **2016**, *125*, 185–188. [[CrossRef](#)]
132. Liu, S.; Li, G.; Qi, Y.; Peng, Z.; Ye, Y.; Liang, J. Corrosion and Tribocorrosion Resistance of MAO-Based Composite Coating on AZ31 Magnesium Alloy. *J. Magnes. Alloy.* **2022**, *10*, 3406–3417. [[CrossRef](#)]
133. Zhang, G.; Wu, L.; Tang, A.; Ding, X.; Jiang, B.; Atrens, A.; Pan, F. Smart Epoxy Coating Containing Zeolites Loaded with Ce on a Plasma Electrolytic Oxidation Coating on Mg Alloy AZ31 for Active Corrosion Protection. *Prog. Org. Coat.* **2019**, *132*, 144–147. [[CrossRef](#)]
134. Dou, J.; Wang, J.; Lu, Y.; Chen, C.; Yu, H.; Ma, R.L.-W. Bioactive MAO/CS Composite Coatings on Mg-Zn-Ca Alloy for Orthopedic Applications. *Prog. Org. Coat.* **2021**, *152*, 106112. [[CrossRef](#)]
135. Toorani, M.; Aliofkhaezrai, M.; Naderi, R.; Golabadi, M.; Sabour Rouhaghdam, A. Role of Lanthanum Nitrate in Protective Performance of PEO/Epoxy Double Layer on AZ31 Mg Alloy: Electrochemical and Thermodynamic Investigations. *J. Ind. Eng. Chem.* **2017**, *53*, 213–227. [[CrossRef](#)]
136. Li, Z.; Yang, W.; Yu, Q.; Wu, Y.; Wang, D.; Liang, J.; Zhou, F. New Method for the Corrosion Resistance of AZ31 Mg Alloy with a Porous Micro-Arc Oxidation Membrane as an Ionic Corrosion Inhibitor Container. *Langmuir* **2019**, *35*, 1134–1145. [[CrossRef](#)] [[PubMed](#)]
137. Sun, W.; Liu, Y.; Li, T.; Cui, S.; Chen, S.; Yu, Q.; Wang, D. Anti-Corrosion of Amphoteric Metal Enhanced by MAO/Corrosion Inhibitor Composite in Acid, Alkaline and Salt Solutions. *J. Colloid. Interface Sci.* **2019**, *554*, 488–499. [[CrossRef](#)] [[PubMed](#)]

138. Li, Z.; Yu, Q.; Zhang, C.; Liu, Y.; Liang, J.; Wang, D.; Zhou, F. Synergistic Effect of Hydrophobic Film and Porous MAO Membrane Containing Alkynol Inhibitor for Enhanced Corrosion Resistance of Magnesium Alloy. *Surf. Coat. Technol.* **2019**, *357*, 515–525. [[CrossRef](#)]
139. Liu, S.; Li, Z.; Yu, Q.; Qi, Y.; Peng, Z.; Liang, J. Dual Self-Healing Composite Coating on Magnesium Alloys for Corrosion Protection. *Chem. Eng. J.* **2021**, *424*, 130551. [[CrossRef](#)]
140. Zhang, A.; Liu, C.; Sui, P.; Sun, C.; Cui, L.; Kannan, M.B.; Zeng, R.-C. Corrosion Resistance and Mechanisms of Smart Micro-Arc Oxidation/Epoxy Resin Coatings on AZ31 Mg Alloy: Strategic Positioning of Nanocontainers. *J. Magnes. Alloy.* **2023**. [[CrossRef](#)]
141. Lu, X.; Feng, X.; Zuo, Y.; Zheng, C.; Lu, S.; Xu, L. Evaluation of the Micro-Arc Oxidation Treatment Effect on the Protective Performance of a Mg-Rich Epoxy Coating on AZ91D Magnesium Alloy. *Surf. Coat. Technol.* **2015**, *270*, 227–235. [[CrossRef](#)]

Disclaimer/Publisher's Note: The statements, opinions and data contained in all publications are solely those of the individual author(s) and contributor(s) and not of MDPI and/or the editor(s). MDPI and/or the editor(s) disclaim responsibility for any injury to people or property resulting from any ideas, methods, instructions or products referred to in the content.